CLPB Mutations Cause 3-Methylglutaconic Aciduria, Progressive Brain Atrophy, Intellectual Disability, Congenital Neutropenia, Cataracts, Movement Disorder

Saskia B. Wortmann,[1,*] Szymon Ziętkiewicz,[2,25] Maria Kousi,[3,25] Radek Szklarczyk,[4,25] Tobias B. Haack,[5,6] Søren W. Gersting,[7] Ania C. Muntau,[8] Aleksandar Rakovic,[9] G. Herma Renkema,[1] Richard J. Rodenburg,[1] Tim M. Strom,[5,6] Thomas Meitinger,[5,6] M. Estela Rubio-Gozalbo,[10] Elzbieta Chrusciel,[2] Felix Distelmaier,[11] Christelle Golzio,[3] Joop H. Jansen,[12] Clara van Karnebeek,[13,14] Yolanda Lillquist,[13] Thomas Lücke,[15] Katrin Õunap,[16] Riina Zordania,[16] Joy Yaplito-Lee,[17] Hans van Bokhoven,[18] Johannes N. Spelbrink,[1,19] Frédéric M. Vaz,[20] Mia Pras-Raves,[20] Rafal Ploski,[21] Ewa Pronicka,[22] Christine Klein,[9] Michel A.A.P. Willemsen,[23] Arjan P.M. de Brouwer,[18] Holger Prokisch,[5,6] Nicholas Katsanis,[3] and Ron A. Wevers[24]

We studied a group of individuals with elevated urinary excretion of 3-methylglutaconic acid, neutropenia that can develop into leukemia, a neurological phenotype ranging from nonprogressive intellectual disability to a prenatal encephalopathy with progressive brain atrophy, movement disorder, cataracts, and early death. Exome sequencing of two unrelated individuals and subsequent Sanger sequencing of 16 individuals with an overlapping phenotype identified a total of 14 rare, predicted deleterious alleles in *CLPB* in 14 individuals from 9 unrelated families. *CLPB* encodes caseinolytic peptidase B homolog ClpB, a member of the AAA+ protein family. To evaluate the relevance of CLPB in the pathogenesis of this syndrome, we developed a zebrafish model and an in vitro assay to measure ATPase activity. Suppression of *clpb* in zebrafish embryos induced a central nervous system phenotype that was consistent with cerebellar and cerebral atrophy that could be rescued by wild-type, but not mutant, human *CLPB* mRNA. Consistent with these data, the loss-of-function effect of one of the identified variants (c.1222A>G [p.Arg408Gly]) was supported further by in vitro evidence with the mutant peptides abolishing ATPase function. Additionally, we show that CLPB interacts biochemically with ATP2A2, known to be involved in apoptotic processes in severe congenital neutropenia (SCN) 3 (Kostmann disease [caused by *HAX1* mutations]). Taken together, mutations in *CLPB* define a syndrome with intellectual disability, congenital neutropenia, progressive brain atrophy, movement disorder, cataracts, and 3-methylglutaconic aciduria.

Introduction

The implementation of exome sequencing (ES) and genome sequencing has expanded our knowledge of genes that cause pediatric syndromic phenotypes.[1] For a subset of these individuals, the diagnostic approach can be assisted by findings from metabolic markers in blood and urine that might point toward hitherto unappreciated inborn errors of metabolism (IEMs).[2]

3-methylglutaconic acid (3-MGA) detected in urine samples is such a marker, showing consistently and significantly elevated levels in a rapidly growing group of IEMs with a syndromic phenotype.[3] This group encompasses several disorders in which phospholipid remodeling and other mitochondrial membrane-related processes are defective. Clinical features are heterogeneous but distinctive. For example, Barth syndrome (MIM 302060), caused by mutations in *TAZ* (MIM 300394), is associated with

[1]Nijmegen Centre for Mitochondrial Disorders (NCMD), Amalia Children's Hospital, Radboudumc, 6500HB Nijmegen, the Netherlands; [2]Department of Molecular and Cellular Biology, Intercollegiate Faculty of Biotechnology, University of Gdańsk, Kładki str. 24, 80822 Gdańsk, Poland; [3]Center for Human Disease Modeling, Duke University Medical Center, Durham, NC 27710, USA; [4]Clinical Genomics, Maastricht UMC+, PO Box 616, 6200MD Maastricht, the Netherlands; [5]Institute of Human Genetics, Helmholtz Zentrum Munich, 85764 Neuherberg, Germany; [6]Institute of Human Genetics, Technische Universität München, 81675 Munich, Germany; [7]Department of Molecular Pediatrics, Dr. von Hauner Children's Hospital, Ludwig-Maximilians-University, 80337 Munich, Germany; [8]Department of Pediatrics, University Children's Hospital, University Medical Center Eppendorf, 20246 Hamburg, Germany; [9]Institute of Neurogenetics, University of Lübeck, 23562 Lübeck, Germany; [10]Departments of Pediatrics and Laboratory Genetic Metabolic Diseases, Maastricht University Medical Center, 6202AZ Maastricht, the Netherlands; [11]Department of General Pediatrics, Neonatology and Pediatric Cardiology, University Children's Hospital, Heinrich-Heine University, Moorenstr. 5, 40225 Düsseldorf, Germany; [12]Department of Laboratory Medicine, Laboratory of Hematology, Radboudumc, 6525GA Nijmegen, the Netherlands; [13]Division of Biochemical Diseases, Department of Pediatrics, B.C. Children's Hospital, Treatable Intellectual Disability Endeavour, Vancouver, BC V6H 3N4, Canada; [14]Child and Family Research Institute, Centre for Molecular Medicine & Therapeutics, University of British Columbia, Vancouver, BC V5Z 4H4, Canada; [15]Department of Neuropediatrics, University Children's Hospital, Ruhr University Bochum, 44791 Bochum, Germany; [16]Department of Genetics, United Laboratories, Tartu University Hospital, Tartu 51014, Estonia; [17]Metabolic Genetics, Murdoch Childrens Research Institute, Royal Children's Hospital, Parkville, VIC 3052, Australia; [18]Department of Human Genetics, Donders Institute for Brain, Cognition and Behaviour, Radboudumc, 6500HB Nijmegen, the Netherlands; [19]BioMediTech, University of Tampere, 33014 Tampere, Finland; [20]Department of Clinical Chemistry and Pediatrics, Laboratory Genetic Metabolic Disease, Academic Medical Center, 1100AZ Amsterdam, the Netherlands; [21]Department of Medical Genetics, Warsaw Medical University, 02-106 Warsaw, Poland; [22]Department of Pediatrics, Nutrition and Metabolic Diseases, Department of Medical Genetics, Children's Memorial Health Institute, 20 Aleja Dzieci Polskich, 04-730 Warsaw, Poland; [23]Department of Neurology, Radboudumc, 6500HB Nijmegen, the Netherlands; [24]Department of Laboratory Medicine, Translational Metabolic Laboratory, Radboudumc, 6525GA Nijmegen, the Netherlands
[25]These authors contributed equally to this work
*Correspondence: saskia-wortmann@gmx.de
http://dx.doi.org/10.1016/j.ajhg.2014.12.013.

(cardio)myopathy, neutropenia, and delayed motor milestones; Sengers syndrome (MIM 212350), driven by mutations in *AGK* (MIM 610345), manifests cardiomyopathy and cataracts; and MEGDEL syndrome (MIM 614739), caused by mutations in *SERAC1* (MIM 614725), is associated with deafness and dystonia.[4] In addition, congenital neutropenia and central nervous system involvement have also been reported in disorders without 3-MGA-uria, such as Kostmann syndrome (MIM 610738; *HAX1* [MIM 605998]), Shwachman-Bodian-Diamond disease (MIM 260400; *SBDS* [MIM 607444]), and Cohen syndrome (MIM 216550; *VPS13B* [MIM 607817]).[5]

Here we present a constellation of pathologies that cannot be reconciled with any known clinical entity. This phenotypic spectrum encompasses intellectual disability (ID)/developmental delay (DD), congenital neutropenia, progressive brain atrophy, movement disorder, and bilateral cataracts. Though all individuals share 3-MGA-uria as a characteristic biomarker, the severity of the other signs and symptoms shows interindividual variability. Nonetheless, under the hypothesis that the consistently observed metabolic signature underpins a discrete molecular genetic disorder, we performed ES in two unrelated individuals, followed by subsequent candidate gene testing in a further 16 affected individuals. Through these studies, the implementation of an in vivo model that recapitulated key neuroanatomical aspects of the disorder, and biochemical in vitro testing, we report the identification of loss-of-function mutations in *CLPB* (RefSeq accession number NM_030813.4).

Subjects and Methods

Clinical Cohort

Individuals #6 and #9 manifested an overlapping phenotype of ID, neutropenia, cataracts, and 3-MGA-uria and were independently evaluated by ES at two different centers (RadboudUMC, Nijmegen, the Netherlands; Helmholtz Zentrum Munich, Germany). After identification of the genetic defect in these cases, we selected 16 additional individuals with an overlapping clinical presentation from the internal database at RadboudUMC. This study adhered to the Declaration of Helsinki and written informed consent was obtained from each individual.

Exome Sequencing and Variant Identification

ES for individual 6 was performed as previously described.[6] In brief, we used a SureSelect Human All Exon 50 Mb Kit (Agilent) for enrichment and a HiSeq2500 (Illumina). Reads were aligned to the UCSC human reference assembly (hg19) with BWA v.0.5.8. More than 90% of the exome was covered at least 20×. Single-nucleotide variants (SNVs) and small insertions and deletions were detected with SAMtools v.0.1.7. Variant prioritization was performed based on an autosomal-recessive pattern of inheritance. ES for individual 9 was performed as previously described with minor adjustments.[2] In brief, we used the SureSelectXT Human All Exon 50Mb Kit (Agilent) for enrichment and a SOLiD 5500XL (Life Technologies). We excluded all nongenic, intronic (other than canonical splice sites), and synonymous variants and all known variants with a frequency >1% in dbSNP v.132 and our in-house variant database consisting of 672 exomes. Next, because a recessive disease model was expected and given the assumption of a common ancestral allele (based on parental consanguinity), we prioritized variants according the percentage of variant reads. For this, we used the threshold of >75% variant reads as an indicator for homozygous variants.

Mutation Analysis by Sanger Sequencing

Primer sequences for amplification of all protein coding exons of *CLPB* (RefSeq NM_030813.4) are shown in Table S1 available online. PCR conditions are available upon request. PCR products were sequenced with the ABI PRISM BigDye Terminator Cycle Sequencing v.2.0 Ready Reaction Kit and analyzed with the ABI PRISM 3730 DNA analyzer (Applied Biosystems).

In Vivo Functional Modeling of *CLPB* Mutations in Zebrafish

Zebrafish embryos and adults were maintained and mated as described and all experiments were carried out with the approval of the Institutional Animal Care and Use Committee (IACUC).[7] For the in vivo complementation experiments, a translational-blocking morpholino (MO) against the sole zebrafish *clpb* ortholog was designed (Figure S1) and obtained from Gene Tools. We injected 1 nl of diluted MO (2.5 ng) and/or RNA (200 pg for WT or mutant *clpb*) into wild-type zebrafish embryos at the 1- to 4-cell stage. For acetylated tubulin staining marking the neuronal axon processes, injected embryos were treated as described.[8] For RNA rescue and overexpression experiments, the human wild-type mRNA of the canonical isoform (RefSeq NM_030813.4) of *CLPB* was cloned into the pCS2+ vector and transcribed in vitro with the SP6 Message Machine kit (Ambion). The four variants tested—p.Arg408Gly, p.Met411Ile, p.Tyr617Cys, and p.Gly646Val—were introduced with Phusion high-fidelity DNA polymerase (New England Biolabs) and custom-designed primers. Image acquisition and analysis was performed with Nikon NIS-Elements Advanced Research software. All experiments were repeated in triplicate and significance of the morphant phenotype was judged by Student's χ^2 test.

Purification and Biochemical Characterization of Human CLPB

The CLPBΔN92 construct (deletion of predicted signal peptide) was PCR generated with a pENTR223-hCLPB plasmid as a template. The amplified DNA fragment was cloned into the pET15b vector (Novagen) at the NdeI/BamHI sites, resulting in a construct pET15b-CLPBΔN92 with an introduced N-terminal His-tag. The construct was verified by DNA sequencing. The p.Arg408Gly change of CLPBΔN92 was introduced into pET15b-CLPBΔN92 by site-directed mutagenesis and confirmed by DNA sequencing.

The CLPBΔN92 and its p.Arg408Gly variant were expressed in *E. coli* BL21(DE3). Pelleted cells were diluted 1/1 (v/v) with buffer (NaCl 300 mM, imidazole 20 mM, glycerol 20%, 2-mercaptoethanol 5 mM, HEPES 20 mM [pH 7.4]), French press lysed, and centrifuged at 75,000 × *g* for 1 hr. The lysate was incubated with 2 ml Ni-NTA resin in batch mode. After washing with buffer (NaCl 150 mM, imidazole 20 mM, glycerol 20%, 2-mercaptoethanol 5 mM, HEPES 40 mM [pH 7.4]) and then with the same buffer supplemented with 48 mM imidazole, proteins were eluted with 300 mM pure imidazole and applied on a PD10 desalting column equilibrated with buffer without imidazole (the other components

of washing buffers, elution buffers, and desalting buffers remained the same). Protein identity was confirmed by immunoblot, via an anti-CLPB antibody (Abcam, ab87253) (Figure S2A). Figure S2B shows purified CLPB_WT and the purified CLPB_p.Arg408Gly on SDS-PAGE. Protein concentrations were estimated by Coomassie-stained SDS-PAGE gel densitometry with BSA as a standard. The ATPase activity of purified human wild-type CLPB (CLPB_WT) and its p.Arg408Gly mutant (CLPB_p.Arg408Gly) was analyzed with the coupled pyruvate kinase/lactate dehydrogenase assay, as previously described.[9] 2 μM hCLPB was incubated with 20 mM ATP at 36°C and the absorbance change was recorded at 1 s intervals. The rate was calculated from the linear part of the curve (steady-state rate). For WT hCLPB, the measurement was additionally performed in the presence of casein (0.2 mg/ml).

Results

The Phenotypic Spectrum of Individuals with Mutations in *CLPB*

The clinical presentation and course of the 14 affected individuals (eight females, six males) varied substantially from a mild phenotype (individuals #1 and #2) associated with cataracts and neutropenia but no neurological involvement or infections to the most severe phenotype (individuals #9–#14) associated with neonatal or even prenatal onset of neurological symptoms (progressive brain atrophy, absence of development, movement disorder, seizures), severe neutropenia with progression into leukemia, and death in the first months of life. The detailed clinical histories of the cohort can be found in the Supplemental Data and are summarized in Table 1 and Figures 1 and 2. Common features include ID/DD (12/14 individuals investigated), congenital neutropenia (10/14), brain atrophy (7/9), microcephaly (7/12), movement disorder (7/13), cataracts (5/10), and 3-MGA-uria (12/12 individuals). The oldest affected participant alive is 18 years old and the youngest is 2 years old. Six individuals passed away between the ages of 24 days and 46 months.

Neurological Phenotype

Two individuals (#1 and #2), currently aged 8 and 10 years, showed no neurological involvement at all as determined by a normal neurological examination, normal IQ test, and, in one person, normal brain imaging. However, individual #1 had ADHD, dyslexia, and dysgraphia and individual #2 had a tendency to impulsivity. All other persons (#3–#14) showed DD/ID; the most severe cases (#10–#14) did not develop at all, did not make any eye or other contact, and suffered from (episodic to permanent) unconsciousness from birth until their early death. Most of them (individuals #3–#14) showed pyramidal tract involvement, progressing from severe hypotonia during the first months of life to severe bilateral spasticity thereafter. In the most severe cases (individuals #12–#14), these degenerative processes probably started during fetal life, because all were born as "stiff babies" with generalized increased muscle tension including contractures and jaw lock. Additionally, 11 individuals suffered swallowing difficulties, potentially of both muscular and central nervous origin, necessitating tube feeding. In four individuals, epilepsy was reported. Furthermore, there is a spectrum of MRI abnormalities ranging from isolated cerebellar atrophy (#6, Figure 1J) in less severely affected individuals to atrophy of both cerebral hemispheres, the basal ganglia, and the cerebellum in the most severely affected persons (Figures 1E–1H). Additionally, white matter involvement was seen in individuals #7–#9 and 11. The brain atrophy corresponds with the clinical finding of microcephaly in 7 of 12 investigated persons. In the individuals with basal ganglia involvement (#7–#9), clinically established dystonia was observed.

Hematological/Immunological Phenotype

Neutropenia was noted in 10 of the 14 individuals, as severe (<0.5 g/l) in six (#1, #9–#11, #13, #14) and moderate (0.5–1.0 g/l) in three (#2, #6, #12). One person (#3) was found to be neutropenic only subsequent to infections, the severity of which appear concomitant with the severity of the neurological phenotype. Whereas individuals without neurological symptoms (#1, #2) did not suffer from recurrent infections, individuals #3–#8 suffered from more frequent infections than peers but without serious complications. The remaining individuals from the study cohort (#9–#14) suffered regularly from serious, often life-threatening infections and were treated with G-CSF (#9 and #12, during infections also #3), continuous antibiotics, and antimycotics (see Figure 2A for details on neutropenia of #9). The bone marrow examination of individual #9 showed a maturation arrest at the stage of the promyelocyte (Figures 2B and 2C). In addition, we observed an absence of mature neutrophils in the bone marrow of individuals #10 and #11. Of note, two siblings, who were not treated with G-CSF, progressed to (1) an acute myeloid leukemia (M5, acute monocytic, with the typical finding of a somatic monosomy of chromosome 7; individual #10) or a (2) myelodysplastic syndrome/preleukemia of myelomonocytic type (individual #11), respectively. Chemotherapeutic treatment was initiated in individual #10, who died shortly after. No treatment was initiated in individual #11, who also died shortly after the diagnosis. Bone marrow aspiration in the third available individual (#13) showed a vacuolar degeneration of the phagocytic mononuclear system without typical signs of neutropenia.

Other Signs and Symptoms

For ten of the study participants, information about ophthalmological findings was available. Five of these individuals had bilateral cataracts, and one (#7) was diagnosed with a suspected pigmentary retinopathy. Two individuals showed cardiac involvement, namely mild septal hypertrophy (#7) and mild dilated cardiomyopathy (#14). Two study participants had endocrine abnormalities (#6 and #7). At least three individuals (#9–#11) showed similar facial dysmorphisms (e.g., low nasal bridge, hypertelorism, tented mouth; Figures 1B and 1C). From a biochemical standpoint, no consistently elevated serum

Table 1. Clinical, Biochemical, and Neuroradiological Findings in Individuals with Mutations in *CLPB*

Individual, Gender	Family	ID	Change (aa)	Neutropenia	Generalized Brain Atrophy	Movement Disorder	Muscle Tone	Cataracts	3-MGA-Uria	Current Age	Other
#1, m	1	no	p.Met411Ile and p.Tyr617Cys	CS	ND	–	normal	-	+	10 years	
#2, f	1	no	p.Met411Ile and p.Tyr617Cys	CM	–	–	normal	+	+	8 years	
#3, m	2	moderate	p.Arg408Gly and p.Arg417*	IS	ND	ataxia	floppy infant, mild truncal hypotonia	–	+	5 years 9 months	neonatal hypoglycaemia, microcephaly
#4, m	2	moderate	p.Arg408Gly and p.Arg417*	–	ND	–	floppy infant, mild truncal hypotonia	+	+	2 years 2 months	neonatal hypoglycaemia, microcephaly
#5, f	2	moderate	p.Arg408Gly and p.Arg417*	–	ND	–	floppy infant, mild truncal hypotonia	–	+	2 years 2 months	neonatal hypoglycaemia, microcephaly
#6, f	4	mild	p.Glu435_Gly436delinsAspPro and p.Gly646Val	CM	+[a]	ataxia, dysarthria, tremor	mild tetraspasticity	+	+	18 years	microcephaly, hypothyreoidea, hypergonadotropic hypogonadism
#7, f	5	severe	p.Cys486Arg homozygous	–	+	dystonia	floppy infant, progressive tetraspasticity	+	+	17 years	microcephaly IUGR, epilepsy, hypothyreoidea, mild cardiac septal hypertrophy, nystagmus
#8, f	5	severe	p.Cys486Arg homozygous	–	+	dystonia, athetosis	floppy infant, progressive tetraspasticity	–	+	9 years	microcephaly, epilepsy, nystagmus
#9, f	6	severe	p.Ala591Val homozygous	CS	+	hyperkinesia, dystonia	floppy infant, progressive tetraspasticity	+	+	3 years 10 months[b]	microcephaly, IUGR, neonatal hypoglycaemia, life-threatening drooling
#10, m	7	severe	p.Tyr272Cys and p.Tyr567Cys	CS	+	–	floppy infant, progressive tetraspasticity	ND	ND	3 months[b]	hepatosplenomegaly, leukemia, facial dysmorphism
#11, f	7	severe	p.Tyr272Cys and p.Tyr567Cys	CS	+	–	floppy infant, generalized hypotonia	ND	+	3 months[b]	hepatosplenomegaly, myelodysplastic and preleukemic syndrome, facial dysmorphism
#12, f	8	severe	p.Cys647Leufs*26 and p.Ile682Asn	CM	+	ataxia, tremor	stiff baby	–	+	5 months[b]	microcephaly, IUGR, epilepsy
#13, m	9	severe	p.Arg250*, p.Arg417*, and p.Glu501Lys	CS	ND	jittery	stiff baby	ND	+	24 days[b]	epilepsy
#14, m	9	severe	p.Arg250*, p.Arg417*, and p.Glu501Lys	CS	ND	ND	stiff baby	ND	ND	54 days[b]	IUGR, mild dilated cardiomyopathy

All individuals are of European descent. Abbreviations are as follows: CM, chronic moderate; CS, chronic severe; ID, intellectual disability; IS, intermittent severe; IUGR, intrauterine growth retardation; ND, no data; 3-MGA-uria, 3-methylglutaconic aciduria.
[a]Isolated cerebellar atrophy.
[b]Age deceased.

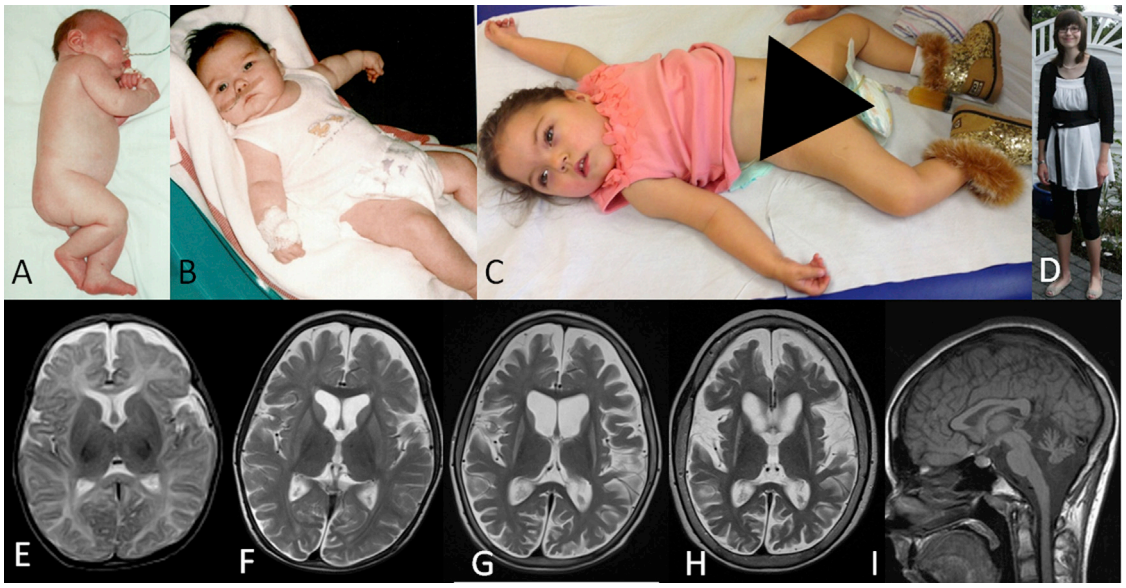

Figure 1. Individual Photographs and MRI Findings
(A) Individual #10 was born with increased muscle tone.
(B and C) Study participants #11 (B) and #9 (C) with tented mouth, hypertelorism, and truncal hypotonia.
(D) Individual #6 displayed no facial dysmorphisms and is able to stand freely.
(E–H) Consecutive T2-weighted MR images of individual #8, axial view, at the age of 2.5 months (E), 16 months (F), 3.5 years (G), and 7 years (H), demonstrating progressive brain atrophy with both cortical and white matter volume decrease over time. Progressive, symmetrical basal ganglia atrophy was supported by abnormally increased T2 signal intensity in the caudate nucleus and putamen starting at the age of 16 months.
(I) Isolated cerebellar atrophy was observed in study participant #6 as determined T1-weighted sagittal MRI.

lactate or alanine levels were observed in any of the investigated individuals, nor did they have an elevated urinary excretion of Krebs cycle intermediates. All individuals had consistent and significant excretion of 3-MGA in their urine, amounting to 2–15 times over the limit of the reference range, pointing to a possible mitochondrial dysfunction. It was observed that the concentration of this biomarker could fluctuate in an individual (#2, 29–109 [reference < 12 μmol/mmol creatinine]; #6, 34–160; and #12, 52–93 [reference < 20]), seemingly without having a direct relation to the clinical condition.

Identification of Mutations in *CLPB* and Mutational Spectrum

For each individual, ES resulted in a list of four to six candidate genes. For individual #6, these were *OBSCN* (MIM 608616), *SCN4A* (MIM 603967), *CEACAM20*, and *CLPB*; and for individual #9, *CLVS2*, *PDZD7* (MIM 612971), *TMEM63C*, *COG7* (MIM 606978), *BAHCC1*, and *CLPB*. Besides being the only overlapping gene, *CLPB* was considered a candidate gene because of the mitochondrial targeting sequence predicting a mitochondrial localization and the previous association of 3-MGA-uria with mitochondrial dysfunction.[10] We detected two heterozygous variants, c.1305_1307inv (p.Glu435_Gly436delinsAspPro) and c.1937G>T (p.Gly646Val) in the coding region of *CLPB* (RefSeq NM_030813.3) for individual #6 while both parents were heterozygous for one of the two variant alleles. In individual #9, a homozygous variant, c.1772C>T (p.Ala591Val), was identified and confirmed to be heterozygous in each of the parents. Given these findings, we performed Sanger sequencing of the entire coding region of *CLPB* in 16 additional subjects that shared phenotypes with our discovery cohort; we identified likely pathogenic *CLPB* mutations in 12 of them, all of which segregated (wherever testing was possible) with the disorder under an autosomal-recessive paradigm.

In total, we identified 14 different *CLPB* mutations (2 nonsense, 1 frameshift, 11 missense; Table 2, Figure 3, Figure S3) in 14 affected individuals from nine independent families of primarily northern European descent (Canada, Australia, Germany, Turkey, Italy, Poland, Estonia). Consistent with a disease-causal role, all variants are either absent or were rare (<0.1% MAF) in the in-house database of 5,036 exomes (Department of Human Genetics, Helmholtz Zentrum, Munich, Germany) and in public databases. The most frequent change, c.1222A>G (p.Arg408Gly), had a MAF of 0.011% in the ExAC browser (detected in 22/122,848 alleles, seen only in heterozygosity and never in homozygosity). The nonsense and frameshift mutations are predicted to result in nonsense-mediated mRNA decay (NMD). Of note, each of the most severely affected individuals (#13 and #14) is compound heterozygous for a nonsense and a missense mutation. Because the parents are unavailable for further research, we could not determine whether these nonsense mutations map on the same haplotype. However, it is tempting to speculate that compound heterozygous

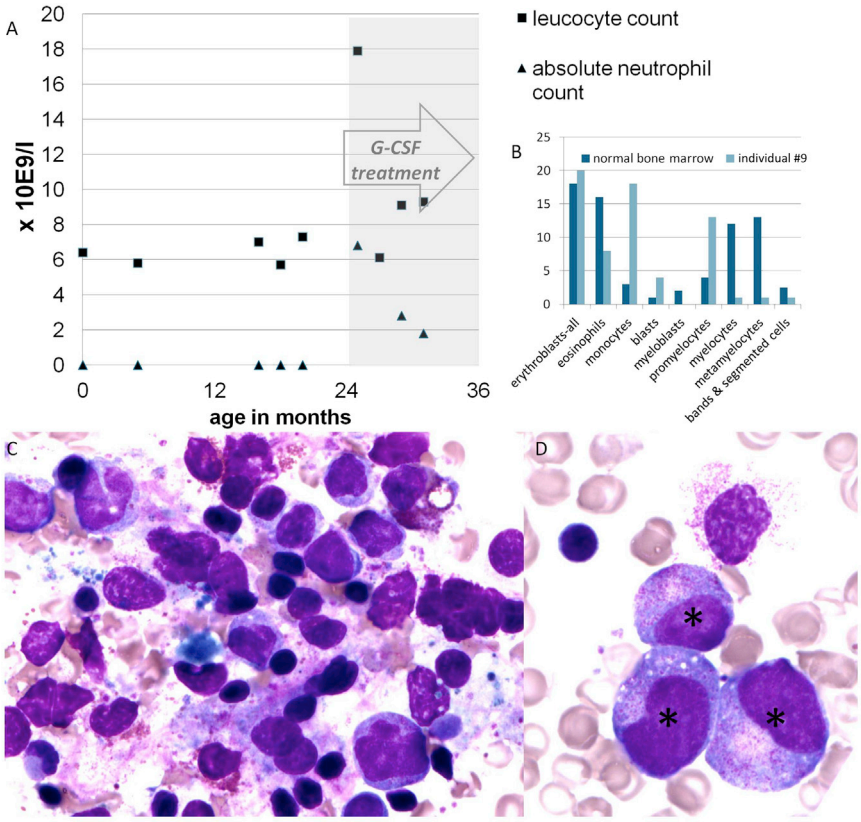

Figure 2. Leucocyte Counts, Images, and Maturation Arrest

(A) Leucocyte (reference range 4.5–10 g/l) and absolute neutrophil count (reference range at birth, 12–15 g/l; 2–12 months, >2 g/l; >12 months, >1.5 g/l) of individual #9 before and during successful treatment with G-CSF.

(B) The total bone marrow composition at 20 months of life of the same individual: blasts 4%, promyelocytes 13%, myelocytes 1%, metamyelocytes 1%, bands and segmented cells 1%, neutrophils 2%, basophils 0%, eosinophils 8%, lymphocytes 32%, monocytes 18%, plasma-cells 0%, normoblasts 20% in comparison with a normal bone marrow.

(C and D) Crista biopsy of individual #9 at 20 months of age shown in two distinct magnifications. The bone marrow contains many promyelocytes (*), but no mature neutrophils (maturation arrest at promyelocyte stage), many macrophages, hemophagocytosis, and atypical lymphocytes.

nonsense mutations result in a more severe phenotype than missense variants. All missense mutations affect amino acids that are evolutionarily conserved across vertebrates and mostly in bacteria (Figure S4). Moreover, all missense mutations are predicted to have a deleterious impact on protein function by different prediction programs (SIFT, PolyPhen, MutationTaster)[11–13] and map to functional domains and the C-tail of CLPB. There was no clear correlation between the severity of the disease and the position and nature of the specific missense mutations. Pathogenic mutations in *CLPB* from this study have been uploaded to the Leiden Open Variation Database (LOVD-*CLPB* page).

CLPB was shown to be expressed in a broad range of human fetal and adult tissues with a significantly higher expression in adult brain tissues (Figure S5). Of note, the expression in fetal brain is approximately five times lower than in adult brain; we also observed low expression in granulocytes.

Evaluation of Mitochondrial Function in Fibroblasts from Affected Individuals

The first 92 amino acid residues of human CLPB are predicted to encode a mitochondrial targeting sequence (MITOPROT).[14] The predicted mitochondrial localization for human CLPB was confirmed by immunofluorescence of CLPB in U2OS cells (Figure S6). Given that other IEMs with 3-MGA-uria as a discriminative feature exhibit mitochondrial dysfunction (e.g., Barth, Sengers, and MEGDEL syndromes), we wondered whether mutations in *CLPB* could affect oxidative phosphorylation.[3,10] We did not detect histological abnormalities, with the exception of a modest dominance of type I fibers, in muscle of individuals #6 and #9. Evaluation of the oxidative phosphorylation in the same individuals in fresh muscle and cultured fibroblasts did not show any abnormalities (Table S3). Finally, autophagy and mitophagy were assessed in cell lines from four individuals, yielding results that were indistinguishable from controls cells (Figure S7). Taken together, these data suggest that *CLPB* mutations are unlikely to affect mitochondrial function in general, or respiratory chain oxidative phosphorylation defects or other dysfunction in particular.

Evaluation of Phospholipid Metabolism

Several of the IEMs with 3-MGA-uria as discriminative feature have been associated with defective phospholipid metabolism. For instance, typical abnormalities in the quantity and acyl-chain composition of cardiolipin (CL), phosphatidylglycerol (PG), and bis(monoacylglycerol) phosphate (BMP) species are characteristic biomarkers in fibroblasts from individuals with Barth and MEGDEL syndromes.[2,4] As such, we investigated the different phospholipid species in fibroblasts from our cohort. Phospholipid analysis of fibroblasts of individuals #1, #3, #6, and #9 showed normal quantity and acyl-chain composition of PG and BMP compared to seven control cell lines (Figure S8). The total amount of CL was lower in affected individuals than in controls (Figure S8). However, the significance level ($p = 0.037$) as well as the difference in total CL amounts was marginal, which might reflect the limited number of data points. No abnormalities were observed in

Table 2. Mutations in *CLPB* and Their Predicted Effects at the Protein Level

Individual	Mutation (nt)	Change (aa)	Exon	Mutation Type	Domains Affected	(Predicted) Effect	Occurence in the ExAC Browser
#13, #14	c.748C>T	p.Arg250*	6	nonsense	all	truncated protein, NMD	not detected
#10, #11	c.815A>G	p.Tyr272Cys	6	missense	ANK	–	2 het / 122918 alleles
#3, #4, #5	c.1222A>G	p.Arg408Gly	11	missense	AAA+	probably affects ATP binding	22 het / 122848 alleles
#1, #2	c.1233G>A	p.Met411Ile	11	missense	AAA+	probably affects ATP binding	not detected
#3, #4, #5, #13, #14	c.1249C>T	p.Arg417*	11	nonsense	AAA+, D2	truncated protein, NMD	4 het / 122824 alleles
#6	c.1305_1307inv	p.Glu435_Gly436delinsAspPro	12	missense	AAA+	likely to affect substrate interaction[30]	not detected
#7, #8	c.1456T>C	p.Cys486Arg	13	missense	AAA+	–	not detected
#13, #14	c.1501G>A	p.Glu501Lys	13	missense	AAA+	–	1 het / 121514 alleles
#10, #11	c.1700A>G	p.Tyr567Cys	15	missense	D2 boundary	–	5 het /122590 alleles
#9	c.1772C>T	p.Ala591Val	16	missense	D2	probably affects stabilization of D2 domain	not detected
#1, #2	c.1850A>G	p.Tyr617Cys	16	missense	D2	probably affects oligomer stabilization	not detected
#6	c.1937G>T	p.Gly646Val	17	missense	D2	–	1 het / 122598 alleles
#12	c.1937dupG	p.Cys647Leufs*26	17	frameshift	D2	truncated protein, NMD	not detected
#12	c.2045T>A	p.Ile682Asn	17	missense	C-tail	–	not detected

Overview of all mutations found in *CLPB* in the different individuals. Abbreviations are as follows: aa, amino acid; het, heterozygous; NMD, nonsense-mediated mRNA decay; nt, nucleotide.

other phospholipid species in the fibroblasts from the four individuals tested (phosphatidic acids, phosphatidylcholines, phosphatidylethanolamines, phosphatidylserines, phosphatidylinositols, cardiolipins, sphingomyelines, and their lyso-analogs; data not shown). Taken together, we found no unambiguous evidence for a general role of CLPB in phospholipid metabolism.

Functional Analysis of Nonsynonymous Variants in *CLPB* by In Vivo Complementation in Zebrafish Embryos

To investigate the pathogenic potential of the nonsynonymous missense *CLPB* alleles identified in our study cohort, we turned to the developing zebrafish as a surrogate model. We first evaluated the effect of the MO-induced knockdown on the cerebellar integrity and the ability of human *CLPB* mRNA to rescue that phenotype in the developing embryos. Among the observed pathologies in individuals with *CLPB* mutations, CNS defects are the most penetrant structural phenotypes (>90% of individuals; Table 1). As such, given that previous studies have demonstrated that cerebellar defects can be modeled in the developing *D. rerio*,[8,15] we focus on this phenotype. We first identified the sole ortholog of *CLPB* in the zebrafish genome by reciprocal BLAST. Because all six exons of the gene were divisible by three, hampering our ability to generate bona fide loss-of-function alleles by inhibiting splicing, we designed a translational blocking morpholino (tbMO). Injection of 2.5 ng of the *clpb* MO resulted in approximately 50% of the injected embryos developing cerebellar defects that ranged in severity from depletion of the axonal connections across the midline of the cerebellum to complete atrophy (Figures 4 and S9). The phenotype was dosage sensitive: progressive increases led to concomitant increase of the penetrance of the cerebellar phenotype to 100% of embryos at 6 ng (Figure S9). The MO-induced phenotype was rescued significantly and reproducibly ($p < 0.0001$; performed in triplicate, scored blind to injection cocktail) by coinjection with 200 pg of human capped *CLPB* mRNA (Figures 4 and S9). By contrast, coinjection of the *clpb* MO with human mRNA encoding each of the four candidate pathogenic variants tested (p.Arg408Gly, p.Met411Ile, p.Tyr617Cys, and p.Gly646Val) were indistinguishable to MO alone (p.Arg408Gly [$p = 0.79$], p.Met411Ile [$p = 0.54$], p.Tyr617Cys [$p = 0.47$], and p.Gly646Val [$p = 0.92$]), suggesting that these variants have little or no residual activity (Figure 4). Overexpression of *CLPB* WT mRNA, or mRNA harboring each of the four variants, had no effect on the cerebellar integrity (Figure S10).

Evaluation of ATPase Function of Human CLPB

We were able to express human CLPB in *E. coli* after removing the mitochondrial targeting sequence and confirm that human CLPB retains ATPase activity (Figure S11). Unlike the bacterial ClpB chaperone, the ATPase activity was not found to be stimulated by the presence of casein, a natively unfolded soluble substrate. We

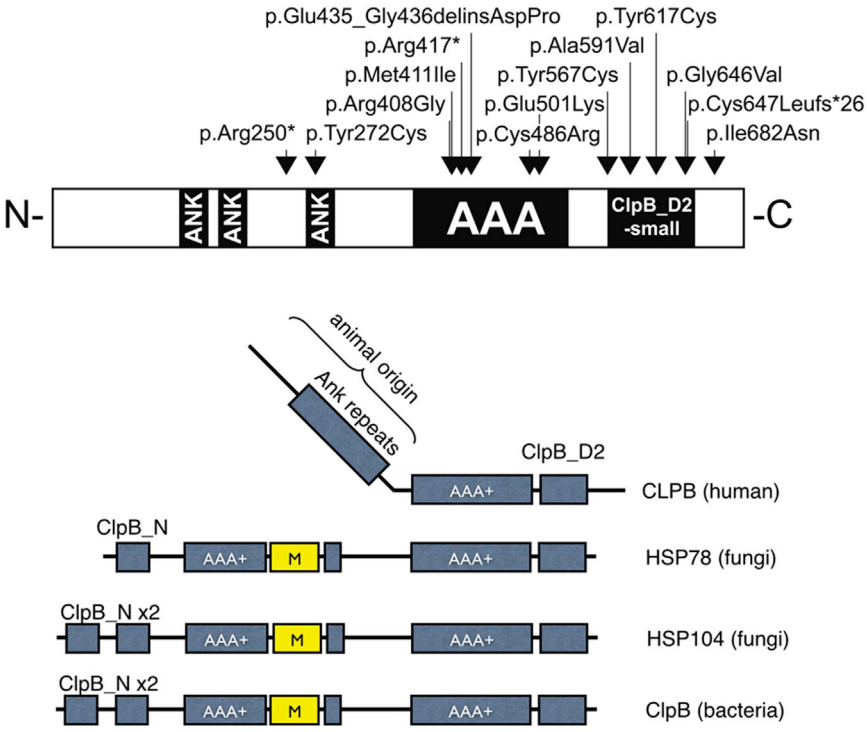

Figure 3. Schematic Representation of CLBP in Human, Fungi, and Bacteria
(A) The positions of all mutations identified in human. Black boxes represent the two main functional domains: the ankyrin domain (ANK) consisting of a short 34 residue repeat implicated in a wide range of protein-protein interactions and the ATPase domain (AAA+).[31,32]
(B) Evolutionary changes in domain composition of CLPB proteins in human, fungi (mitochondrial HSP78 and cytosolic HSP104), and bacteria. All CLPB-family homologs possess at least a single AAA+ domain and the specific CLPB-D2 domain. In contrast to human CLPB, fungi and bacteria possess an "M domain," a ClpB N domain, and an additional AAA+ domain. Ankyrin repeats are present only in the human homolog and are probably species specific.

also expressed the mutant CLPB_p.Arg408Gly (found in individuals #3–#5) in *E. coli*. This change in the AAA+ domain of CLPB is at the interface between the CLPB oligomers and in the vicinity of the ATP binding site and hence is predicted to influence the ATPase activity through impaired ATP binding. Consistent with this prediction, the ATPase activity level of the mutant protein is 26% of that of wild-type human CLPB in *E. coli* (Figure S11).

Protein Interaction Network for CLPB and HAX1

A database search resulted in 17 proteins with an established physical interaction with CLPB. The live-cell screen of CLPB against a library of 100 proteins by means of bioluminescence resonance energy transfer (BRET) identified 19 additional direct interactions (Tables S4 and S5). For HAX1, a total of 38 protein interactions was listed in the BioGRID database. Within the networks of first-order protein interactions for both proteins, a link between CLPB and HAX1 is established by mutual interaction with the sarcoplasmic/endoplasmic reticulum Ca^{2+}-ATPase (*ATP2A2* [MIM 108740]).

Discussion

Here we present our clinical and molecular genetic analyses of a cohort of individuals, the phenotype(s) of which cannot be reconciled with any known clinical entity. The phenotypic spectrum encompasses ID/DD, congenital neutropenia, progressive brain atrophy, movement disorder, and bilateral cataracts. Though all individuals share 3-MGA-uria as a characteristic biomarker, the severity of the other signs and symptoms described shows interindividual variability. On aggregate, however, we propose that our cohort represents a distinct clinical entity that leads to an encephalopathy predominantly involving gray matter, which can start as early as in fetal life, as well as chronic moderate to severe neutropenia due to a maturation arrest at the promyelocyte stage. We do not know whether these pathologies are related. However, we note that individuals with the more attenuated neurological phenotypes also had the more severe hematologic disease, which proceeded to leukemia in two siblings. The broad phenotypic spectrum cannot be reconciled readily by the underlying genotype. However, we note that the individuals with the most severe phenotypes (#12–#14) also carry disease-causing variants predicted to lead to the complete absence of functional protein. Given the observed clinical variability, we speculate that other genetic as well as environmental factors (e.g., infections) could exacerbate the clinical presentation.

Under the hypothesis that the consistently observed metabolic signature underpins a discrete molecular genetic disorder, we performed ES in two unrelated individuals, followed by subsequent candidate gene testing in an additional 16 affected individuals. Through these studies we identified 14 independent mutations in *CLPB* in 14 individuals from 9 unrelated families. Taken together, our data suggest that *CLPB* is the major locus for this phenotype, although additional genes are likely to exist. We further supported these claims by developing a zebrafish model of the disorder, in which we recapitulated key aspects of the neuroanatomical phenotypes of the affected individuals. Specifically, embryos bereft of endogenous *clpb* show microcephaly, reduction of the size of the optic tectum (OT; a structure equivalent to the superior culiculus in humans), and degeneration of the axons forming

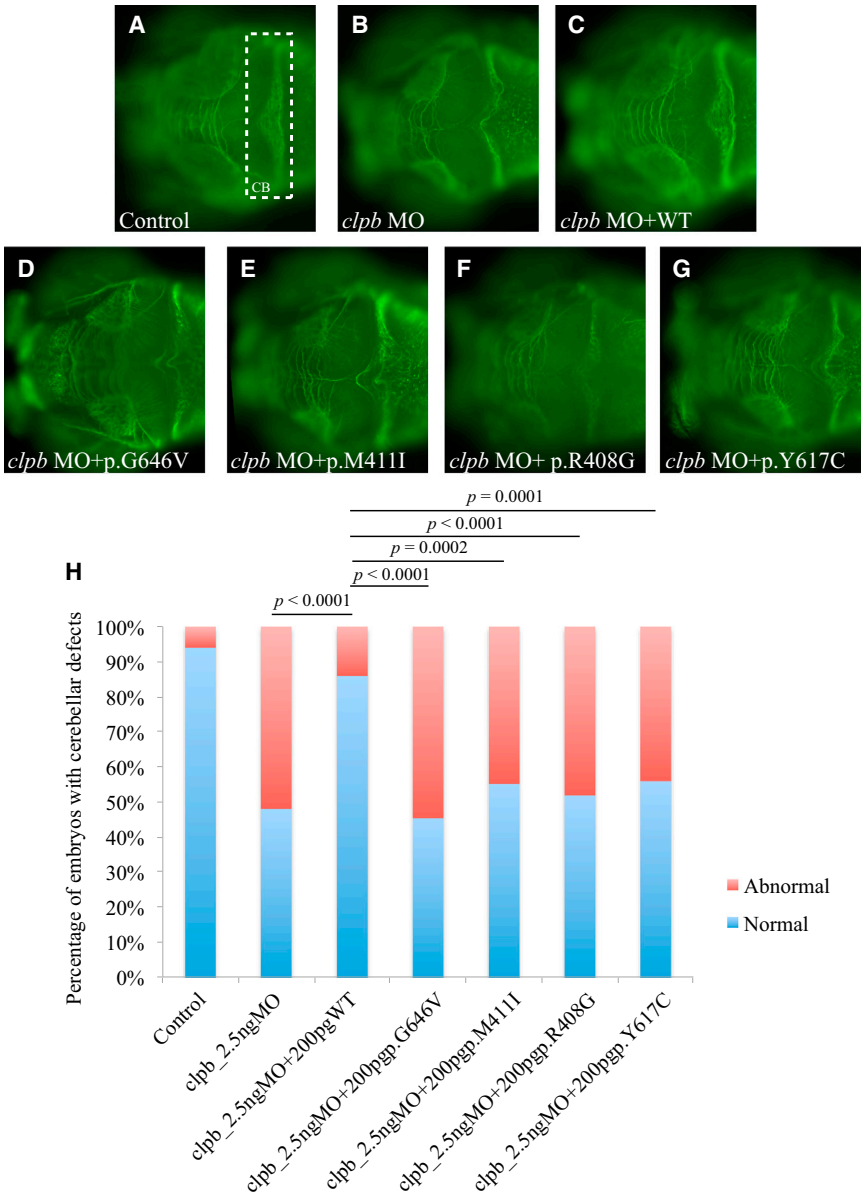

Figure 4. The CLPB Zebrafish Model
In vivo complementation of four CLPB variants (p.Arg408Gly, p.Met411Ile, p.Tyr617Cys, and p.Gly646Val) identified in evaluated study participants, in zebrafish.
(A–G) Dorsal view of the developing zebrafish brain stained with acetylated tubulin at 3 days postfertilization (dpf). The cerebellum (CB) is highlighted by a white dashed rectangle in (A) showing a control embryo.
(A–C) Control (A), morpholino injection (B), and rescue (C) by human WT mRNA.
(D–G) Illustration of the effects of the tested alleles.
(H) Graphic representation of the scoring for CB defects in control and injected embryos. Coinjection of MO with WT human *CLPB* mRNA results is a statistically significant reduction in the number of embryos with cerebellar defects ($p < 0.0001$). By contrast, coinjection of MO with each of the human *CLPB* mRNAs carrying the four mutations tested score as pathogenic being indistinguishable from the MO-injected embryos.

the cerebellum, reminiscent of the clinical features in the individuals with *CLPB* mutations. Additionally, coinjection of the *clpb* MO with human mRNA bearing each of the four detected in our cohort alleles tested were indistinguishable to MO alone, suggesting that these alleles have little or no residual activity and that the observed syndromic phenotypes in humans are driven by null or near null mutations in all cases studied. It will be important to generate genetic *clpb* mutants to study the progression and molecular pathology of these phenotypes, as well as the possible manifestation of other phenotypes, such as cataracts, that are found in some but not all individuals with *CLPB* mutations. Likewise, it will be critical to accumulate additional individuals with *CLPB* mutations and ascertain whether mutations that retain partial protein function correlate with an attenuated phenotype, or indeed any phenotype at all.

CLPB belongs to the large AAA+ (ATP-ases associated with diverse cellular activities) superfamily. AAA+ proteins usually form ring-shaped homo-hexamers.[16] Members of this superfamily typically have one or two highly conserved ATPase domains and are involved in various processes, such as DNA replication and repair and protein disaggregation and refolding, and operate as part of dynein motors, as chelatases or proteases.[17] The unifying characteristic of this family of proteins consists in the hydrolysis of ATP through the AAA+ domain to produce energy required to exert mechanic force onto their substrates. The human CLPB protein is characterized further by the presence of a specific C-terminal D2 domain (PFAM identifier PF10431), which is typical for AAA+ proteins involved in polypeptide chain threading through the hexamer central channel. Proteins with this domain form the subfamily of Caseinolytic peptidase (Clp) proteins, also called HSP100 (Heat shock proteins 100 kDa).[18] The human CLPB protein was named after its high homology to the C-terminal part of bacterial ClpB protein which, in cooperation with Hsp70, is involved in the process of disaggregation of protein aggregates and hence is called a disaggregase. Bacterial ClpB proteins dissolve protein aggregates and rescue aggregated proteins by assisting them to fold back into a native, biologically active form.[19] What distinguishes the human CLPB protein from its microbial and plant paralogs is

primarily the domain composition. These microbial orthologs contain an additional AAA+ domain and a small N-terminal domain (Figure 3) and have an "M domain," necessary for disaggregation. Another feature characteristic of the human CLPB is the presence of ankyrin repeats instead of the first of two ATPase domains found in bacteria and fungi, which are used commonly as protein-protein interaction platforms (Figure 3).[20,21] The species-specific presence of the ankyrin repeats in the N-terminal part of the human protein might have evolved to ensure a more elaborate or more refined substrate recognition, to mediate the interaction with as yet unknown protein partners, or even to support a putative chaperone function. Despite the fact that only one of the two ATPase domains is retained in the human CLPB, its presence is postulated to be sufficient to mediate the use of ATP hydrolysis energy for threading unfolded polypeptide through the central channel of the hexamer ring.[22]

Consistent with this hypothesis, we were able to confirm in vitro the ATPase activity of human CLPB. Furthermore, we were able to show that upon the presence of the p.Arg408Gly variant (detected in individuals #3–#5) that is predicted to affect the ATP binding capability of human CLPB, the ATPase activity measured was diminished. Despite the convergence of human and bacterial CLPB proteins on several aspects of molecular function, unlike the bacterial counterpart, the human CLPB cannot be stimulated by casein.

Comparison of the clinical and genetic pathology of individuals with *CLPB* mutations is likewise informative. Mutations in *CLPB* lead to a congenital neutropenia syndrome comparable to Kostmann disease, driven by mutations in *HAX1*, which encodes HCLS1-associated protein X-1 (HAX1).[23] Both disorders can show neurological involvement, which seems, however, to be more severe in individuals with *CLPB* mutations. In individuals with *HAX1* mutations, neurological involvement (epilepsy, ID) can be appreciated only when both *HAX1* isoforms A and B are affected.[24] Despite the variability of neurological symptoms in the two syndromes, remarkable mimicry exists from a hematological standpoint, with individuals affected by either one of the two disorders displaying maturation arrest of the neutrophils at the promyelocyte stage upon bone marrow examination.[25] Furthermore, individuals with either *CLPB* or *HAX1* mutations also exhibit disease progression from neutropenia into leukemic pictures in the absence of GCSF.[26]

Biochemical analyses have established a role of HAX1 in stabilizing the mitochondrial membrane potential and preventing apoptosis via interaction with the mitochondrial proteases presenilin-associated rhomboid-like (PARL), HtrA serine peptidase 2 (HTRA2), and BCL2-associated X protein (Bax).[23,26,27] Further evidence for an antiapoptotic role of HAX1 stems from the observation that it interacts with and downregulates the protein level of the sarco/endoplasmic reticulum Ca^{2+}-ATPase (SR Ca(2+)-ATPase 2 encoded by *ATP2A2*), which regulates the endoplasmic reticulum Ca^{2+} concentration.[28] Evaluation of the protein interaction networks of CLPB predict a biochemical interaction between CLPB and SR Ca(2+)-ATPase 2 (Figure 5; for method, see Table S5), which allows us to speculate that the effect of *CLPB* mutations on hematopoesis could be driven by excessive apoptosis, as is the case in Kostmann syndrome.

To enrich our understanding of the *CLPB*-mutation-mediated disease pathomechanisms, we reasoned that CLPB defects might have an effect on lipid biosynthesis and metabolism, similar to what is observed in Barth syndrome, one of the IEMs with 3-MGA-uria as a discriminative feature, characterized by neutropenia as well as (cardio)myopathy and delayed motor milestones.[29] Despite extensive analysis of the levels of various phospholipids, we detected no involvement of lipid biosynthesis, turnaround, and metabolism in the pathogenesis mediated by mutations in *CLPB*. We also were unable to detect overt abnormalities in mitophagy or autophagy in cells from individuals with *CLPB* mutations. In aggregate, our data argue that despite the clinical mimicry between CLPB disease and Barth syndrome or other IEMs with 3-MGA-uria as a discriminative feature, the mechanisms underlying each condition are diverse.

In conclusion, we describe an as yet unknown inborn error of metabolism with 3-MGA-uria as discriminative feature (CLPB defect). Underlying mutations were found in *CLPB* and lead to a broad phenotypic spectrum encompassing ID/DD, congenital neutropenia, progressive brain atrophy, movement disorder, and bilateral cataracts. The function of human CLPB is currently poorly described but our data show that it might be related to apoptosis.

Accession Numbers

The databank accession number for the data reported in this paper is http://www.lovd.nl/clpb.

Supplemental Data

Supplemental Data include full case reports on the individuals in this paper and describe the mild, moderate, and the severe phenotypes of the disease, additional method descriptions, 11 figures, and 5 tables and can be found with this article online at http://dx.doi.org/10.1016/j.ajhg.2014.12.013.

Acknowledgments

We thank the individuals and their parents for participation in this study. The study was financially supported by Van Leersumfonds, Koninklijke Nederlandse Akademie van Wetenschappen (project VLF2013277 to S.B.W.), by the Dutch society for the study of inborn errors of metabolism (ESN stimulatie beurs to S.B.W.), the NARSAD Young Investigator Grant from BBRF (to C.G.), the Canadian Institutes of Health Research (#301221 grant to C.v.K.), NIH P50MH094268 (to N.K.), the German Bundesministerium für

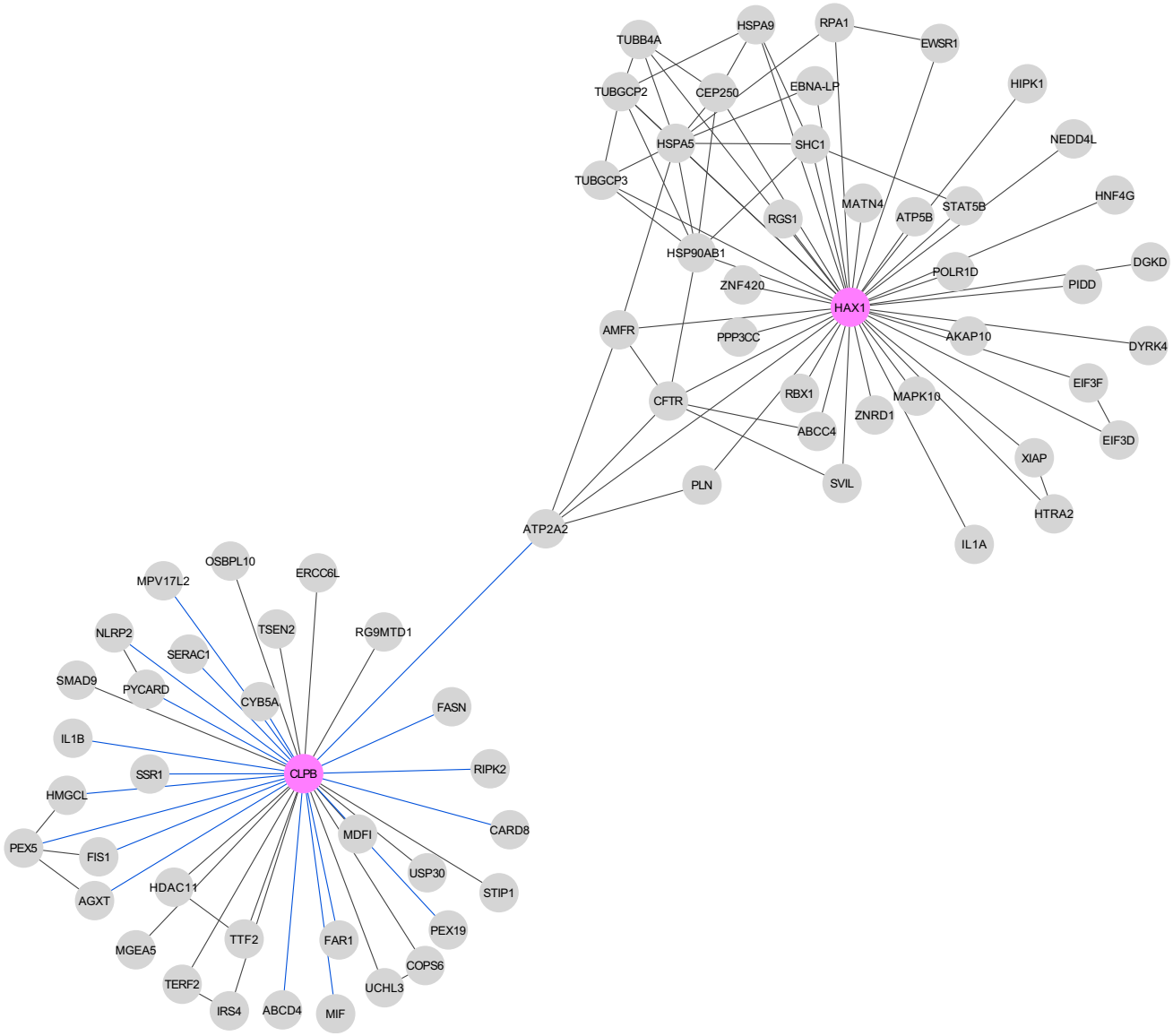

Figure 5. Protein Interaction Network for CLPB and HAX1
A database search resulted in 17 proteins with an established physical interaction with CLPB. The live-cell screen of CLPB against a library of 100 proteins by means of bioluminescence resonance energy transfer (BRET) identified 19 additional direct interactions (Tables S4 and S5). For HAX1, a total of 38 protein interactions were listed in the BioGRID database. Within the networks of first-order protein interactions for both proteins, a link between CLPB and HAX1 is established by mutual interaction with the sarcoplasmic/endoplasmic reticulum Ca^{2+}-ATPase (SR Ca^{2+}-ATPase 2 encoded by *ATP2A2*).

Bildung und Forschung (BMBF) through the German Network for mitochondrial disorders (mitoNET; 01GM1113C to T.M. and H.P.), and through the E-Rare project GENOMIT (01GM1207 for T.M. and H.P.). N.K. is a Distinguished George W. Brumley Professor. C.K. is the recipient of a career development award from the Hermann and Lilly Schilling Foundation and is supported by a grant from the Deutsche Forschungsgemeinschaft (DFG). C.v.K. is the recipient of a scholar award from the Michael Smith Foundation for Health Research. R.S. is financially supported by the Metakids Foundation. We thank Edwin van Kaauwen and Liesbeth Wintjes (Radboudumc Nijmegen) for excellent technical assistance, Dr. Graham Sinclair (University of British Columbia) for providing biochemical data, and Dirk Klee (Heinrich-Heine University) for the MRI images of individual #8. We thank Han Brunner (Radboudumc Nijmegen), K. Liberek (Department of Molecular and Cellular Biology, University of Gdańsk, Poland), Angela Luyf and Antoine van Kampen (AMC, Amsterdam), and Mathias Woidy and Philipp Guder (Ludwig-Maximilians-University, Munich, Germany), as well as Harry Kampinga (University Medical Center Groningen, Groningen, Germany) for fruitful discussions.

Received: November 17, 2014
Accepted: December 10, 2014
Published: January 15, 2015

Web Resources

The URLs for data presented herein are as follows:

BioGRID, http://thebiogrid.org/

Burrows-Wheeler Aligner, http://bio-bwa.sourceforge.net/
dbSNP, http://www.ncbi.nlm.nih.gov/projects/SNP/
ExAC Browser, http://exac.broadinstitute.org/
HPRD, http://www.hsls.pitt.edu/obrc/index.php?page=URL1055173331
LOVD, http://databases.lovd.nl/shared/genes/CLPB
MINT, http://databib.org/repository/602
MitoProt, http://ihg.gsf.de/ihg/mitoprot.html
MutationTaster, http://www.mutationtaster.org/
NHLBI Exome Sequencing Project (ESP) Exome Variant Server, http://evs.gs.washington.edu/EVS/
Online Mendelian Inheritance in Man (OMIM), http://www.omim.org/
PolyPhen-2, www.genetics.bwh.harvard.edu/pph2/
RefSeq, http://www.ncbi.nlm.nih.gov/RefSeq
SAMtools, http://samtools.sourceforge.net/
SIFT, http://sift.bii.a-star.edu.sg/
STRING 9.0, http://www.string-db.org/
UCSC Genome Browser, http://genome.ucsc.edu

References

1. Acehan, D., Xu, Y., Stokes, D.L., and Schlame, M. (2007). Comparison of lymphoblast mitochondria from normal subjects and patients with Barth syndrome using electron microscopic tomography. Lab. Invest. *87*, 40–48.
2. Wortmann, S.B., Vaz, F.M., Gardeitchik, T., Vissers, L.E., Renkema, G.H., Schuurs-Hoeijmakers, J.H., Kulik, W., Lammens, M., Christin, C., Kluijtmans, L.A., et al. (2012). Mutations in the phospholipid remodeling gene *SERAC1* impair mitochondrial function and intracellular cholesterol trafficking and cause dystonia and deafness. Nat. Genet. *44*, 797–802.
3. Wortmann, S.B., Duran, M., Anikster, Y., Barth, P.G., Sperl, W., Zschocke, J., Morava, E., and Wevers, R.A. (2013). Inborn errors of metabolism with 3-methylglutaconic aciduria as discriminative feature: proper classification and nomenclature. J. Inherit. Metab. Dis. *36*, 923–928.
4. Wortmann, S.B., Espeel, M., Almeida, L., Reimer, A., Bosboom, D., Roels, F., de Brouwer, A.P., and Wevers, R.A. (2014). Inborn errors of metabolism in the biosynthesis and remodelling of phospholipids. J. Inherit. Metab. Dis. Published online September 2, 2014. http://dx.doi.org/10.1007/s10545-014-9759-7.
5. Donadieu, J., Fenneteau, O., Beaupain, B., Mahlaoui, N., and Chantelot, C.B. (2011). Congenital neutropenia: diagnosis, molecular bases and patient management. Orphanet J. Rare Dis. *6*, 26.
6. Haack, T.B., Gorza, M., Danhauser, K., Mayr, J.A., Haberberger, B., Wieland, T., Kremer, L., Strecker, V., Graf, E., Memari, Y., et al. (2014). Phenotypic spectrum of eleven patients and five novel MTFMT mutations identified by exome sequencing and candidate gene screening. Mol. Genet. Metab. *111*, 342–352.
7. Niederriter, A.R., Davis, E.E., Golzio, C., Oh, E.C., Tsai, I.C., and Katsanis, N. (2013). In vivo modeling of the morbid human genome using *Danio rerio*. J. Vis. Exp. *78*, e50338.
8. Margolin, D.H., Kousi, M., Chan, Y.M., Lim, E.T., Schmahmann, J.D., Hadjivassiliou, M., Hall, J.E., Adam, I., Dwyer, A., Plummer, L., et al. (2013). Ataxia, dementia, and hypogonadotropism caused by disordered ubiquitination. N. Engl. J. Med. *368*, 1992–2003.
9. Nørby, J.G. (1988). Coupled assay of Na+,K+-ATPase activity. Methods Enzymol. *156*, 116–119.
10. Wortmann, S.B., Kluijtmans, L.A., Rodenburg, R.J., Sass, J.O., Nouws, J., van Kaauwen, E.P., Kleefstra, T., Tranebjaerg, L., de Vries, M.C., Isohanni, P., et al. (2013). 3-Methylglutaconic aciduria—lessons from 50 genes and 977 patients. J. Inherit. Metab. Dis. *36*, 913–921.
11. Ng, P.C., and Henikoff, S. (2003). SIFT: Predicting amino acid changes that affect protein function. Nucleic Acids Res. *31*, 3812–3814.
12. Adzhubei, I.A., Schmidt, S., Peshkin, L., Ramensky, V.E., Gerasimova, A., Bork, P., Kondrashov, A.S., and Sunyaev, S.R. (2010). A method and server for predicting damaging missense mutations. Nat. Methods *7*, 248–249.
13. Schwarz, J.M., Rödelsperger, C., Schuelke, M., and Seelow, D. (2010). MutationTaster evaluates disease-causing potential of sequence alterations. Nat. Methods *7*, 575–576.
14. Claros, M.G., and Vincens, P. (1996). Computational method to predict mitochondrially imported proteins and their targeting sequences. Eur. J. Biochem. *241*, 779–786.
15. Matsui, H., Namikawa, K., Babaryka, A., and Köster, R.W. (2014). Functional regionalization of the teleost cerebellum analyzed in vivo. Proc. Natl. Acad. Sci. USA *111*, 11846–11851.
16. Neuwald, A.F., Aravind, L., Spouge, J.L., and Koonin, E.V. (1999). AAA+: A class of chaperone-like ATPases associated with the assembly, operation, and disassembly of protein complexes. Genome Res. *9*, 27–43.
17. Snider, J., Thibault, G., and Houry, W.A. (2008). The AAA+ superfamily of functionally diverse proteins. Genome Biol. *9*, 216.
18. Zolkiewski, M. (2006). A camel passes through the eye of a needle: protein unfolding activity of Clp ATPases. Mol. Microbiol. *61*, 1094–1100.
19. Rosenzweig, R., Moradi, S., Zarrine-Afsar, A., Glover, J.R., and Kay, L.E. (2013). Unraveling the mechanism of protein disaggregation through a ClpB-DnaK interaction. Science *339*, 1080–1083.
20. Mosavi, L.K., Cammett, T.J., Desrosiers, D.C., and Peng, Z.Y. (2004). The ankyrin repeat as molecular architecture for protein recognition. Protein Sci. *13*, 1435–1448.
21. Li, J., Mahajan, A., and Tsai, M.D. (2006). Ankyrin repeat: a unique motif mediating protein-protein interactions. Biochemistry *45*, 15168–15178.
22. Weibezahn, J., Tessarz, P., Schlieker, C., Zahn, R., Maglica, Z., Lee, S., Zentgraf, H., Weber-Ban, E.U., Dougan, D.A., Tsai, F.T., et al. (2004). Thermotolerance requires refolding of aggregated proteins by substrate translocation through the central pore of ClpB. Cell *119*, 653–665.
23. Klein, C., Grudzien, M., Appaswamy, G., Germeshausen, M., Sandrock, I., Schäffer, A.A., Rathinam, C., Boztug, K., Schwinzer, B., Rezaei, N., et al. (2007). HAX1 deficiency causes autosomal recessive severe congenital neutropenia (Kostmann disease). Nat. Genet. *39*, 86–92.
24. Germeshausen, M., Grudzien, M., Zeidler, C., Abdollahpour, H., Yetgin, S., Rezaei, N., Ballmaier, M., Grimbacher, B., Welte, K., and Klein, C. (2008). Novel HAX1 mutations in patients with severe congenital neutropenia reveal isoform-dependent genotype-phenotype associations. Blood *111*, 4954–4957.
25. Kostmann, R. (1956). Infantile genetic agranulocytosis; agranulocytosis infantilis hereditaria. Acta Paediatr. Suppl. *45* (105), 1–78.

26. Yetgin, S., Olcay, L., Koç, A., and Germeshausen, M. (2008). Transformation of severe congenital neutropenia to early acute lymphoblastic leukemia in a patient with HAX1 mutation and without G-CSF administration or receptor mutation. Leukemia *22*, 1797.
27. Chao, J.R., Parganas, E., Boyd, K., Hong, C.Y., Opferman, J.T., and Ihle, J.N. (2008). Hax1-mediated processing of HtrA2 by Parl allows survival of lymphocytes and neurons. Nature *452*, 98–102.
28. Vafiadaki, E., Arvanitis, D.A., Pagakis, S.N., Papalouka, V., Sanoudou, D., Kontrogianni-Konstantopoulos, A., and Kranias, E.G. (2009). The anti-apoptotic protein HAX-1 interacts with SERCA2 and regulates its protein levels to promote cell survival. Mol. Biol. Cell *20*, 306–318.
29. Houtkooper, R.H., Turkenburg, M., Poll-The, B.T., Karall, D., Pérez-Cerdá, C., Morrone, A., Malvagia, S., Wanders, R.J., Kulik, W., and Vaz, F.M. (2009). The enigmatic role of tafazzin in cardiolipin metabolism. Biochim. Biophys. Acta *1788*, 2003–2014.
30. Leidhold, C., von Janowsky, B., Becker, D., Bender, T., and Voos, W. (2006). Structure and function of Hsp78, the mitochondrial ClpB homolog. J. Struct. Biol. *156*, 149–164.
31. Letunic, I., Doerks, T., and Bork, P. (2014). SMART: recent updates, new developments and status in 2015. Nucleic Acids Res. Published online October 9, 2014. http://dx.doi.org/10.1093/nar/gku949.
32. Sedgwick, S.G., and Smerdon, S.J. (1999). The ankyrin repeat: a diversity of interactions on a common structural framework. Trends Biochem. Sci. *24*, 311–316.

The American Journal of Human Genetics

Supplemental Data

Mutations in *CLPB* Cause Intellectual Disability, Congenital Neutropenia, Progressive Brain Atrophy, Movement Disorder, Cataracts, and 3-Methylglutaconic Aciduria

Saskia B. Wortmann, Szymon Ziętkiewicz, Maria Kousi, Radek Szklarczyk, Tobias B. Haack, Søren W. Gersting, Ania C. Muntau, Aleksandar Rakovic, G. Herma Renkema, Richard J. Rodenburg, Tim M. Strom, Thomas Meitinger, M. Estela Rubio-Gozalbo, Elzbieta Chrusciel, Felix Distelmaier, Christelle Golzio, Joop H. Jansen, Clara van Karnebeek, Yolanda Lillquist, Thomas Lücke, Katrin Õunap, Riina Zordania, Joy Yaplito-Lee, Hans van Bokhoven, Johannes N. Spelbrink, Frédéric M. Vaz, Mia Pras-Raves, Rafal Ploski, Ewa Pronicka, Christine Klein, Michel A.A.P. Willemsen, Arjan P.M. de Brouwer, Holger Prokisch, Nicholas Katsanis, and Ron A. Wevers

Supplemental information

Supplemental case reports

1. Mild phenotype (cataracts, neutropenia, no ID/DD, no movement disorder, no MRI abnormalities)

Individual 1 came to medical attention at 18 months of age with fever and skin infection requiring antibiotics. Severe neutropenia (0.1 G/L) was noted. His neutrophil counts varied (0.1 – 1.1 G/L) in the further course, but he never experienced any infections nor required antibiotics since then. When his younger sister, **individual 2,** was born with bilateral nuclear cataracts, and also showed neutropenia (0.7 G/L) both individuals were evaluated further. Their development and growth until the age of 10 and eight years, respectively, is normal. Both recently had an extensive psychological examination including an IQ assessment, which yielded scores in the average range. The brother was further diagnosed with attention deficit hyperactivity disorder (ADHD), dyslexia and dysgraphia and the sister with a tendency to impulsivity. Though no radiological data are available for individual 1, the MRI of individual 2 at the age of eight years was normal.

2. Moderate phenotype (cataracts, neutropenia, infections, congenital hypotonia progressing to spasticity, mild to severe ID/DD, movement disorder, increasing severity of MRI abnormalities)

Individual 3 presented with intra-uterine growth restriction (IUGR) but showed catch up growth to birth weight p10, length p50, head circumference p3. Bilateral talipes were noted on prenatal ultrasound. The newborn period was complicated by generalized hypotonia, feeding difficulties, and one episode of hypoglycaemia. He underwent serial casting and an achilles tenotomy for talipes. He has intermittent left esotropia and amblyopia with normal fundi, but no cataracts. Since the age of ten months he had recurrent episodes of neutropenia (0.04 G/L) in the context of febrile illnesses but has responded well to short courses of G-CSF. His development is globally delayed. Currently, at the age of 5 years nine months, he has mild truncal hypotonia, is able to walk independently but with a stooped posture and ataxic gait. He is able to spell his name and speak in simple sentences. He has short stature (p10) and microcephaly (p2). Echocardiography is normal.

The proband has a younger brother, **individual 4,** and sister, **individual 5** (uncomplicated twin pregnancy). The boy had generalized hypotonia, more prominent than his twin sister.

Both had problems with hypoglycaemia and poor feeding. At seven months of age, bilateral cataracts were detected in the male individual, which were removed surgically. Ophthalmological investigations in the girl were normal. At 18 months microcephaly became apparent in both children. Both affected individuals remain hypotonic and although they continue gaining skills, their development is globally delayed. At 21 months of age, they are able to sit independently and to crawl. They babble and are able to indicate what they want. Neither twin has had documented febrile neutropenic episodes to date. Echocardiography, hearing assessment and cranial ultrasound were normal.

Individual 6 was evaluated for developmental delay and tremor from the age of 17 months onwards. She has bilateral cataracts and chronic moderate neutropenia (0.6-0.9 G/L) but did not suffer recurrent infections beside *Salmonella* infection at 17 years of age. Hypothyroidism and hypergonadotropic hypogonadism were treated with hormonal substitution. She is now 18 years old and finished regular school with some support. Upon neurologic examination she shows normal head circumference, mild bilateral spasticity and severe cerebellar ataxia, dysarthria and tremor. She can walk with assistance and has no swallowing problems. MRI examination showed progressive, isolated, cerebellar atrophy **(Figure 1I).**

At the age of three months, muscular hypotonia, poor eye contact and uncoordinated eye movements were noted in the female **individual 7**. On eye examination a salt and pepper pigmentation pattern was observed, but no cataracts were observed. At the age of two years swallowing problems necessitated gastrostomy. From the age of four years seizures were noted. Eye-examination at that age was normal apart from strabismus (no cataract, no optic atrophy, no salt and pepper pigmentation). From the age of seven years onwards progressive athetosis and dystonia were noted as well as progressive spasticity of the legs. Serial MRI's up to the age of ten years showed progressive cerebral, cerebellar and basal ganglia atrophy and white matter involvement. An echocardiography at the age of 12 years revealed mild septal hypertrophy. Additionally, hypothyroidism was noted. **Individual 8** is the female cousin of individual 7 and shows an identical course of disease with additional epilepsy. Both individuals never showed neutropenia. The radiological findings of individual 8 are presented in **(Figure 1E-H).**

3. Severe phenotype (neutropenia, cataracts, infections, total lack of development, three individuals with fetal disease, early death and possible development of leukaemia)

Individual 9 was born prematurely at 35 weeks of gestation (wg) and pregnancy was complicated by IUGR. At birth severe generalized hypotonia, bilateral cataracts, a low nasal

bridge, hypertelorism and a tented mouth were noted **(Figure 1C).** She suffered severe drooling and recurrent airway infections as well as otitis media (e.g. pseudomonas aeroguinosa). Chronic severe neutropenia (0.0-0.4 G/L) was noted from the age of three months onwards. Her bone marrow showed maturation arrest at promyelocyte state **(Figure 2).** Continuous treatment with antibiotics, antimycotics and G-CSF as well as gastrostomy and extirpation of saliva glands helped stabilize her clinical condition. She displayed marked developmental delay, never learnt to roll over or to make contact. She had dystonic movements of the hands, feet and perioral and increasing muscle tone of the lower limbs and died at nearly four years of age due to increasing obstructive and central respiratory problems. Her MRI showed cerebellar hypoplasia (the vermis being more affected than the cortical hemispheres) and alterations in globus pallidus and capsula interna as well as white matter alterations in the parieto-occipital region. Evaluation of the oxidative phosphorylation system in fresh muscle and fibroblasts showed no abnormalities.

Individual 10 was born prematurely (35wg). Since birth he had sucking and swallowing difficulties and recurrent vomiting. At the age of 11 days he was hospitalized with clinical signs of sepsis. Since the second week of life severe neutropenia (<0.5 G/L), monocytosis, and recurrent bacterial infections were noticed. He needed tube feeding due to bulbar paralysis and absent swallowing reflexes. Dysmorphic features were noticed involving high and hairy forehead, hypertelorism, low nasal bridge, retrognathia, dysplastic ears, clinodactyly of the hands and hypospadias, partial T2-3 syndactyly **(Figure 1A).** He had absolute developmental arrest; made no eye or other contact. Brain MRI revealed generalized brain atrophy. At the age of two months hepatosplenomegaly, progressive granulocytopenia and monocytosis were noted, and acute myeloid leukemia (phenotype M5; acute monocytic) was diagnosed. The morphological investigation of bone marrow aspirate showed predominantly dysplastic monocytes and dysplastic granulopoiesis. The karyotype from bone marrow cells was 46,XY(95%)/45,XY,-21/45XY,-7. Chemotherapy was initiated, but after the second course the individual deceased at 3.5 months of age. Upon brain autopsy generalized atrophy and polygyria were noted. His younger sister, **individual 11,** was born normally at term and showed identical dysmorphic features, and an identical course of disease with jaundice and group B streptococcal septicemia at day 3 of life. The same dysmorphic features with her brother were noted **(Figure 1B).** She made no eye contact or showed any development. Brain MRI showed generalized brain atrophy and delayed myelination. She had very weak swallowing and sucking reflexes necessitating tube feeding. Furthermore, she suffered progressive severe neutropenia (<0.5 G/L), monocytosis (33-70%) and hepatomegaly from

birth onwards. Bone marrow morphological investigation and immuno-phenotyping was performed three times. There was a predominance of atypical dysplastic monocytes (33-74%), mature neutrophils were almost absent and 10-15% of blasts cells were present. Myelodysplastic syndrome and pre-leukaemic syndrome were diagnosed with a possibility of myelomonocytaric leukaemia. Following the wish of parents she received only palliative care and died at 3.5 months of age. No autopsy was performed.

Individual **12** had *in utero* complications including IUGR, decreased placental flow and polyhydramnion and manifested fetal oedema. From the first day of life, significantly increased muscle tension and jaw clenching were noticed ("stiff baby"). Massive limb tremor, generalized seizures resistant to anticonvulsants, and non-epileptic periodical apnea and unconsciousness were observed and persisted through life. Brain ultrasound, ocular fundus examination and neonatal hearing screening were normal. During the neonatal period the girl presented with increasing respiratory failure and feeding problems for which she received parenteral/tube feeding and transiently assisted ventilation. She had severe chronic neutropenia (0.1-0.7 10E9/l) and suffered severe bacterial and fungal infections despite treatment with antibiotics, antimycotics and G-CSF. Bone marrow biopsy showed vacuolar degeneration of the phagocytic mononuclear system (without typical signs of known congenital neutropenia). She showed hardly no development until passing away at five months of age due to an infection with consecutive cardiorespiratory failure. On autopsy microcephaly, marked loss of cellular structures in both hemispheres of the brain and a total depletion of cellular structures of the cerebellum and brainstem were reported.

The pregnancy with **individual 13** was complicated by placental calcifications, polyhydramnion and IUGR and ended at term by Caesarian section due to fetal distress. The newborn period was dominated by signs of respiratory failure, pneumonia and severe leukopenia. The individual presented tetraspasticity and forced flexion of the limbs, furthermore lockjaw (“stiff baby”), nystagmus and trembling of limbs. He died at months of age. The pregnancy of his younger brother, **individual 14,** was complicated by intrauterine jitteriness / seizures. From birth onwards the individual was jittery, unconscious, non reactive, made no contact and showed severe hypertonia (“stiff baby”). Echocardiographic examination revealed mild dilated cardiomyopathy. Head ultrasound showed abnormal brain structures, no details were reported. Additionally, from the 3rd week of life oliguria appeared followed by generalized oedema. Laboratory studies included persistent leukopenia reaching 1.2 G/L with lymphocythosis. Despite intensive medical treatment, the individual passed away at 24 days of age.

Supplemental figures and tables

Figure S1. Schematic representation of the *D. rerio clpb* locus.

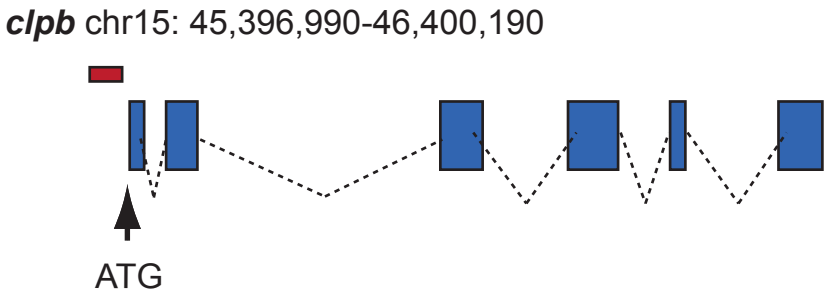

Blue, exons; dashed lines, introns; white, untranslated regions; red box, MO; ATG indicates the translation initiation site.

Figure S2. Preparations of CLPB protein and its p.Arg408Gly (p.R408G) variant.

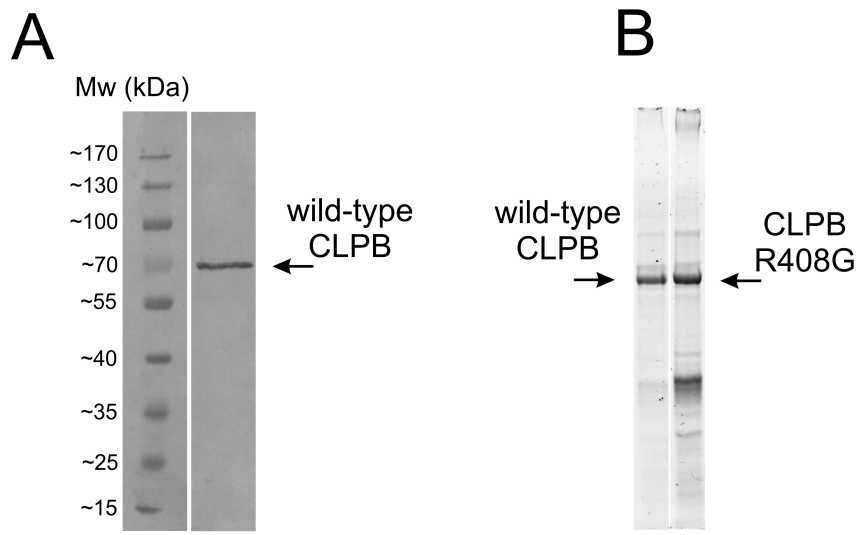

(A) Western blot of purified wild type CLPB protein with an anti-CLPB antibody (Abcam ab87253). B) SDS-PAGE of purified wild type and p.Arg408Gly CLPB sample (Biorad 12% TGX StainFree FastCast gel, visualised with Biorad ChemiDoc MP).

.

Figure S3. CLPB modeling.

Residues affected by missense mutations in the predicted CLPB protein structure (cyan). Two neighboring subunits (magenta and green) are shown, together with the position of the three subunits in the CLPB hexamer (insert). The structural model shown is based on *T. thermophilus* ClpB (pdb:1qvr) and prepared using and PyMOL (www.pymol.org) [20].

Figure S4. Conservation of the mutated CLPB amino acids in the individuals with *CLPB* mutations.

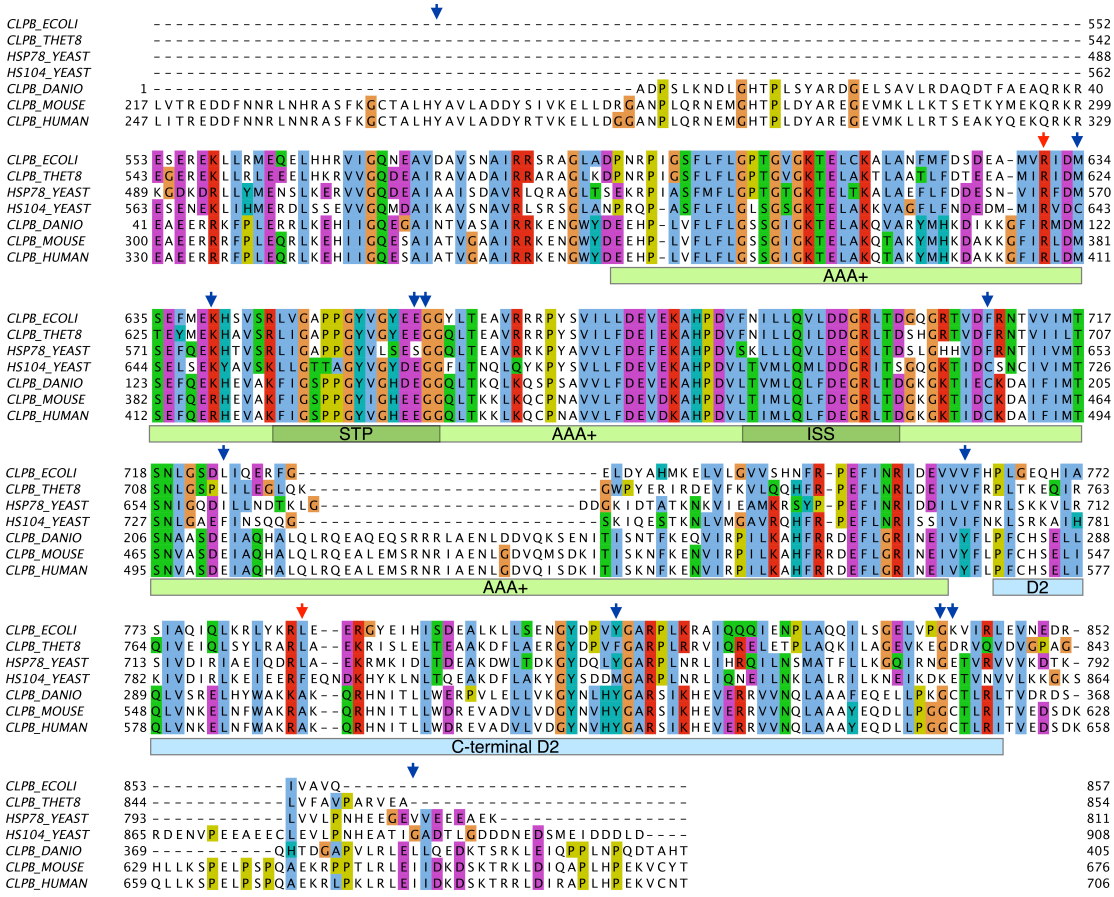

Alignment of the conserved region of human CLPB protein with its bacterial (*E. coli* and *T. thermophilus*), fungal (mitochondrial HSP78 and cytosolic HSP104) as well as vertebrate orthologs [zebrafish (*Danio rerio*) and mouse (*Mus musculus*)]. Arrows denote missense mutations in our cohort of individuals (blue: heterozygous, red: homozygous). Protein domains in the human sequence are marked under the alignment. AAA+ - ATPase domain, C-terminal D2 - CLPB-specific domain not present in other proteins from CLPA/C/X families. The C-terminal domain is essential for oligomerization, stabilizing the functional assembly [21; 22]. Structural motifs are highlighted in the alignment: STP - Substrate Translocation Pore (ISS - Inter-Subunit Signaling) motifs regulating ATP power-stroke for substrate translocation [23; 24]. The total length of the sequences is given in parentheses.

Figure S5. Expression of *CLPB* by mRNA expression analysis in human fetal and adult tissues.

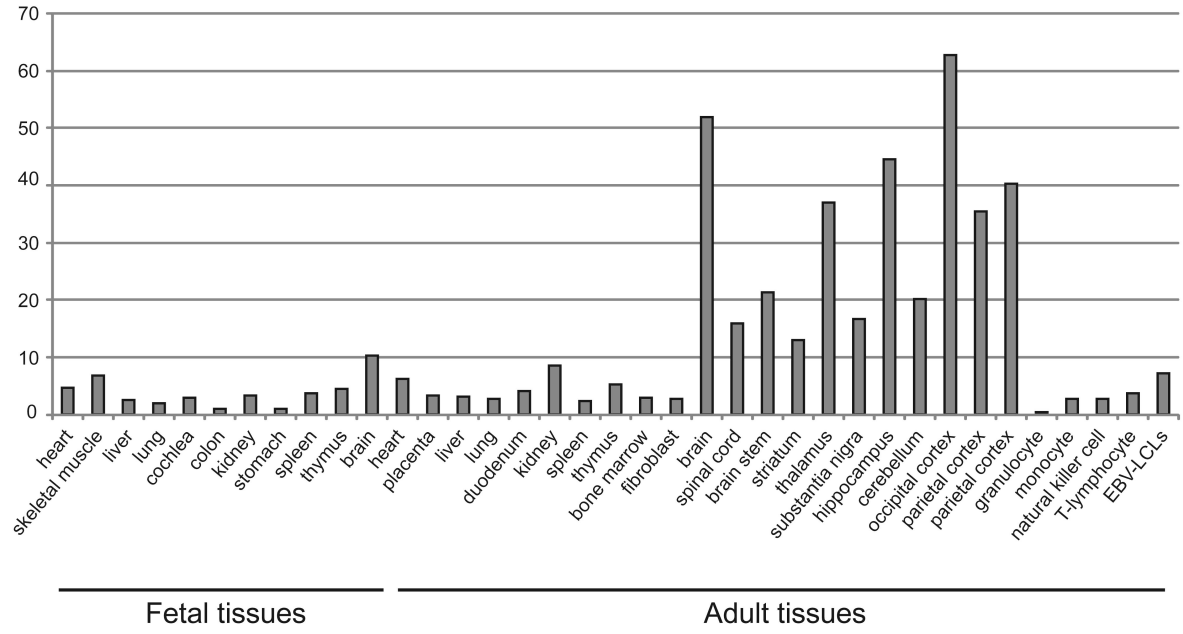

Total RNA from different human adult and fetal tissues was ordered from Stratagene Europe (Amsterdam, The Netherlands). All fetal tissues are from 20 or 21 week-old embryos after gestation, except for cochlear RNA that was isolated from an 8 week-old embryo by using the NucleoSpin RNA II kit (Macherey-Nagel, Düren, Germany) according to the manufacturer's protocols. To remove residual traces of genomic DNA, the cochlear RNA was treated with DNase I (Invitrogen, Leek, The Netherlands) while bound to the RNA binding column. Of all tissues, 5 µg of total RNA were transcribed into cDNA by using the iScript cDNA synthesis kit (Bio-Rad Laboratories, Hercules, CA, USA) according to the manufacturer's protocol. cDNA was purified by using the NucleoSpin extract II kit (Macherey-Nagel, Düren, Germany) according to the manufacturer's protocol. QPCR quantifications were performed in duplicate on the equivalent of 12.5 ng total RNA input. Experimental threshold cycles (Ct) values were within the range of cDNA dilutions used to validate the primers. The melt curves of all PCR products showed a single PCR product. All water controls were negative. GUSB (MIM #611499) and PPIB (MIM# 123841) were used as reference genes. Differences in expression between tissues were calculated by the comparative Ct or $2^{\Delta\Delta Ct}$ method [25; 26]. Relative expression levels are given as the fold change in comparison to the tissue with the lowest expression level.

Figure S6. Subcellular localization of CLPB.

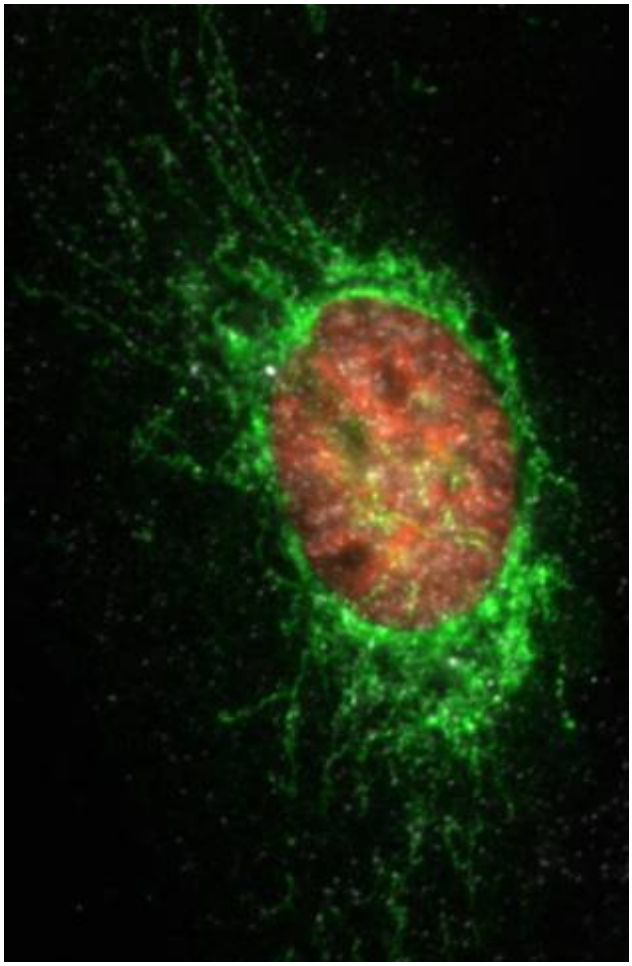

U2OS cells were transiently transfected with CLPB-V5 and pTagRFP-histone H2B expression constructs. CLPB-V5 (green) as well as HSP60 (white) were detected by immunofluorescence and showed mitochondrial co-localization distinct from the nuclear H2B fluorescence (red).

For immunofluorescent detection of V5 tagged CLPB, U2OS cells were grown on coverslips in six well plates and transiently transfected with a pLenti-CLPB-V5 expression construct using TransIT-LT1 (Mirus, Madison, WI) according the manufacturer's instructions. As a transfection efficiency control we co-transfected with a pTagRFP-H2B (Evrogen). The medium was replaced 4 hrs post-transfection with regular cell culture medium. Cells were fixed using 3.3% paraformaldehyde in cell culture medium for 15 min, washed 3x in PBS and permeabilized for 15 min with 0.5% Triton X100 in PBS/10% fetal calf serum (FCS). Primary V5 monoclonal antibody was diluted 1:100 and incubated in PBS/10%FCS for 1 hr. Secondary goat-anti-mouse IgG AlexaFluor 488 was likewise

incubated for 1 hr at a 1:1000 dilution. Slides were mounted using ProLong® Gold antifade with DAPI (Invitrogen). Image acquisition was performed using a Zeiss Observer.Z1with led illumination and appropriate emission filters.

Figure S7. Autophagy flux and mitochondrial clearance. (A, B, C)

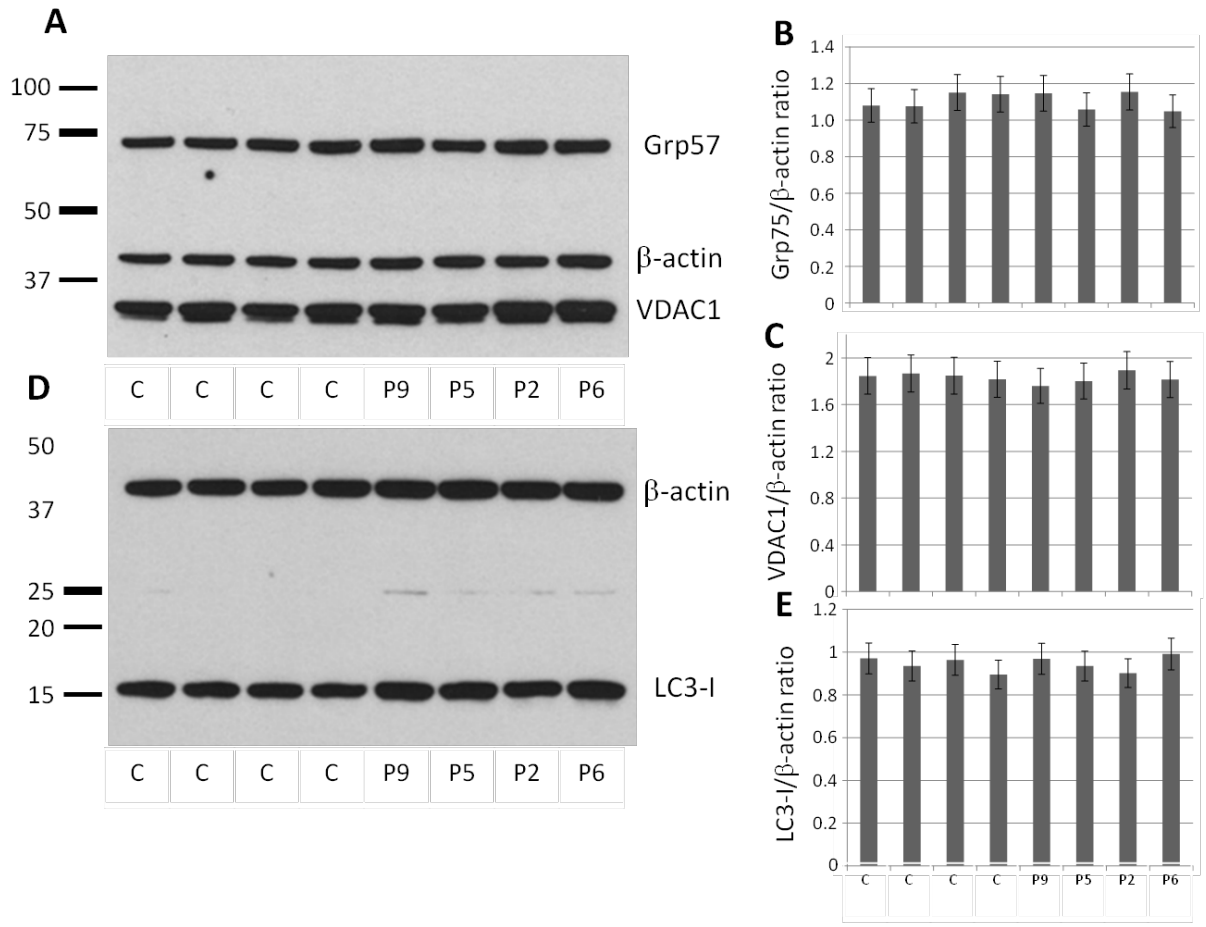

Mitochondrial clearance or mitophagy in fibroblasts under basal conditions was evaluated by measuring the mitochondrial proteins Grp75 and VDAC1 after immuno-blotting on SDS gels. β-Actin served as a loading control. Evidence for the presence or absence of mitophagy was based on the ratio of the two mitochondrial markers over β-actin in four individual cell lines (#9, 5, 2, 6) and four controls. No significant differences were observed. (D, E) Autophagy in fibroblasts was measured under basal conditions. We used the conversion of LC3 from its cytosolic form LC3-I (~17kDa) to the autophagy-relevant form LC3-II (~15kDa), a commonly used indicator of autophagy. The LC3 forms were separated on SDS gels and after immunoblotting expressed as ratio over β-actin using densitometry. No significant differences were found using four affected individual cell lines (#9, 5, 2 and 6) and 4 controls.

Fibroblasts that were used for assessment of mitophagy and autophagy, were kept in high glucose Dulbecco's Modified Eagle's Medium supplemented with 10% FCS (Lonza, Breda, The Netherlands) and 1% 10 U/µl Penicillin-10 µg/µl Streptomycin (Gibco, Breda, The Netherlands). All fibroblasts were grown at 5% CO2 and a temperature of 37°C.

In all assays, fibroblast passage numbers (<10) were matched. To challenge cellular processes of mitophagy by increasing the amount of dysfunctional mitochondria, fibroblasts were treated with the potassium ionophore valinomycin (1µM for 1h, Sigma-Aldrich, St. Louis, CA, USA). Proteins were extracted using RIPA buffer (50mM Tris-HCl pH7.6, 150mM NaCl, 1% DOC, 1% NP-40) containing 0.1% SDS. Cells were dissolved in the appropriate amount of buffer and incubated on ice for 30 min. Next, lysates were centrifuged at 16,000xg for 20min at 4oC. The supernatant was transferred into a new tube and used for Western blotting. Western blot analysis was performed as previously published using antibodies raised against β-actin (1:1000000, #A2228, Sigma-Aldrich, St. Louis, CA, USA), GRP75 (1:1000000, #ab2799, Abcam, Cambridge, UK), LC3 (1:1000, #4108, Cell Signaling Technology, Boston, MA, USA)[2].

Figure S8. Phospholipid analysis in fibroblasts of controls and individuals with the CLPB defect.

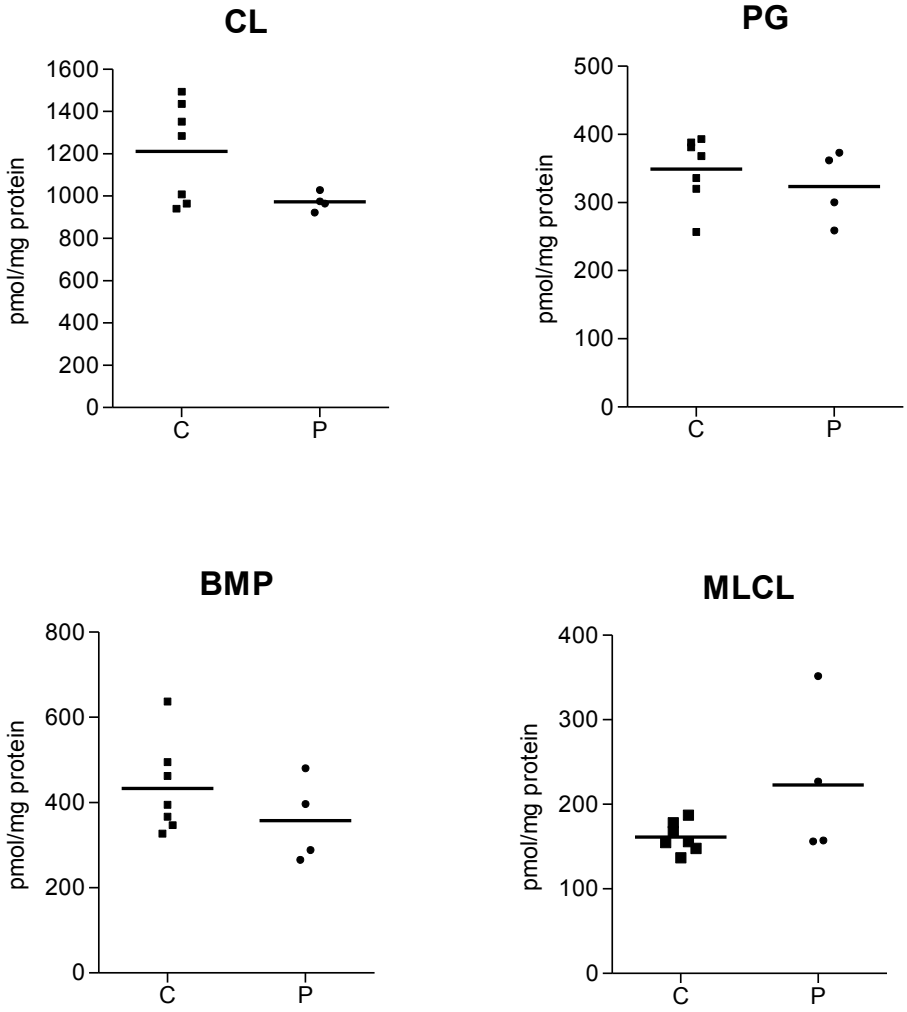

Scatter plots of the total levels of cardiolipin (CL), phosphatidylglycerol (PG), bis(monoacylglycerol)phosphate (BMP) and monolyso-cardiolipin (MLCL) in fibroblasts from controls ("C"; n=7) and affected individuals ("P"; n=4).

Statistical significance was assessed using a two-tailed student's t-test (CL (p=0.037), MLCL (p=0.273), PG (p=0.467) and BMP (p=0.283).

Fibroblast cell lines for phospholipid analysis were cultured in RPMI 1640 medium (Gibco, Breda, The Netherlands) containing 10% (v/v) fetal calf serum (FCS; Sigma, Zwijndrecht, The Netherlands), 1% 10 U/µl Penicillin-10 µg/µl Streptomycin (Gibco, Breda, The Netherlands), and 1% GlutaMAX (Gibco, Breda, The Netherlands). They were harvested by centrifugation at 200xg for 5 min at room temperature, washed once with PBS, pelleted by

centrifugation at 200xg for 5 min at room temperature, and snap frozen in liquid nitrogen. Levels of the following phospholipids were analyzed: PG, BMP, CL and phosphatidic acid (PA), phosphatidylcholine (PC), phosphatidylethanolamine (PE), phosphatidylserine (PS) phosphatidylinositol (PI), sphingomyeline (SM) and their lyso-analogue species. The relative abundances of the species in the sample-extracts were determined by HPLC-MS/MS using a Surveyor HPLC system hyphenated to a TSQ Quantum AM tandem mass spectrometer (Thermo Finnigan Corporation, San Jose, CA, USA). The MS was operated alternating in the negative- and positive ion electrospray ionization (ESI) mode in consecutive runs as described in detail previously [3]. Acyl-chain compositions were determined by the product-ion scans of the respective *quasi* molecular ions.

Figure S9. CNS disorganization upon translation blocking morpholino in the CLPB zebrafish model.

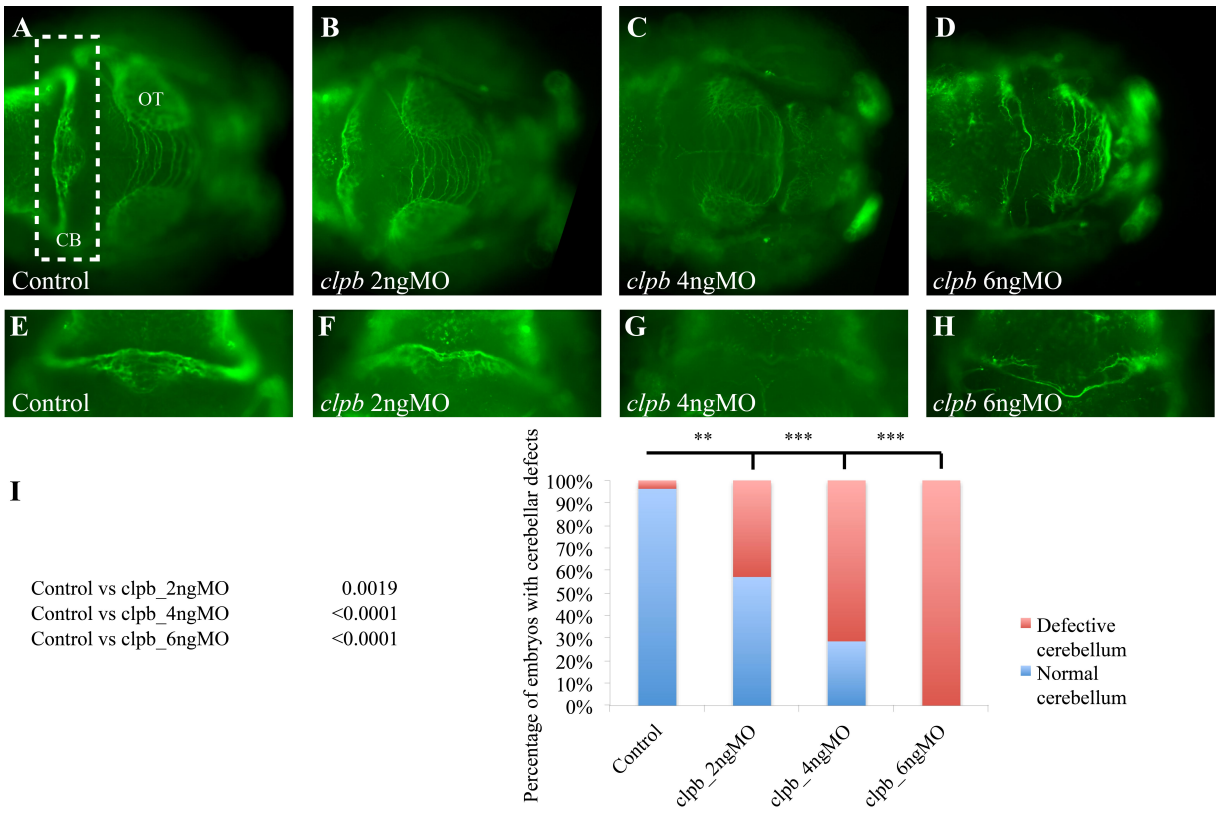

(A-D) Dorsal view of the brain stained with acetylated tubulin in 3 days post fertilization (dpf) in developing zebrafish embryos. A progressive disorganization of the CNS is observed with increasing doses of a translation-blocking morpholino (MO) against *clpb* (TB-*clpb*). More specifically, embryos injected with higher doses of MO show microcephaly, reduction of the size of the optic tectum (OT; a structure equivalent to the superior culliculus in humans), and degeneration of the axons forming the cerebellum (CB). (E-H). Magnifications of the cerebellum, highlighted with the white dashed line in panel A. (I) p-values and quantification of the embryos showing defects in the cerebellum across progressively increasing doses of MO.

Figure S10. Overexpression of the non-synonymous *CLPB* alleles tested with the *in vivo* functional model.

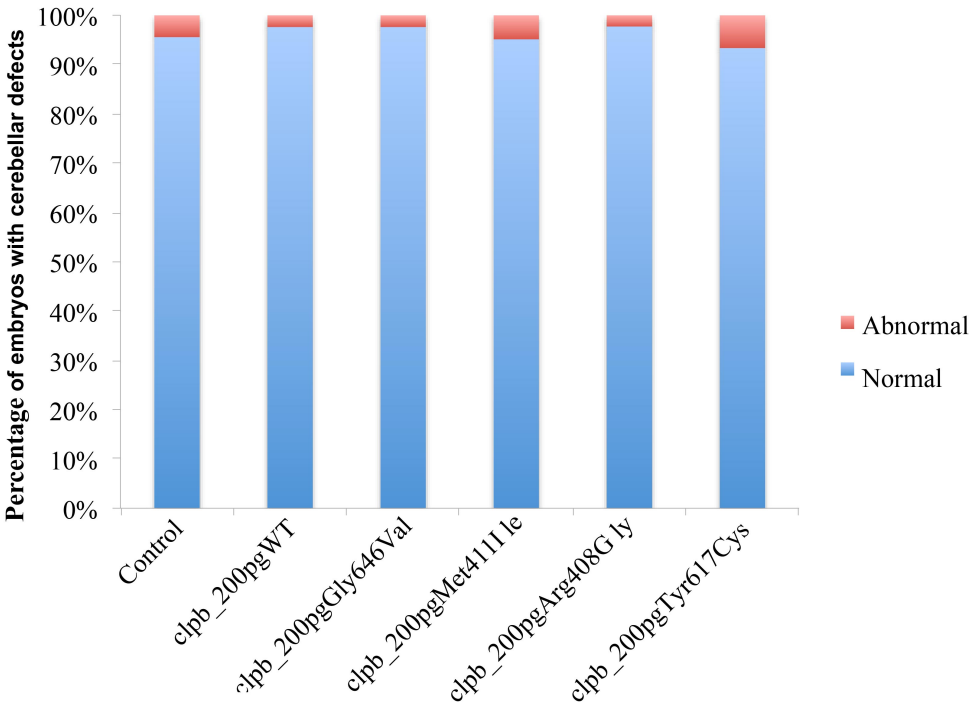

Overexpression of wt *CLPB* mRNA or *CLPB* mRNA harboring any of the variants identified in the study cohort (p.Arg408Gly, p.Met411Ile, p.Tyr617Cys and p.Gly646Val) does not lead to changes in the integrity of the cerebellum in zebrafish embryos at 72 hpf, suggesting that injection of each of the mutant constructs alone does not lead to toxicity and induction of a phenotype similar to the morpholino.

Figure S11. ATPase activity of purified wildtype and p.Arg408Gly (p.R408G) ClpB.

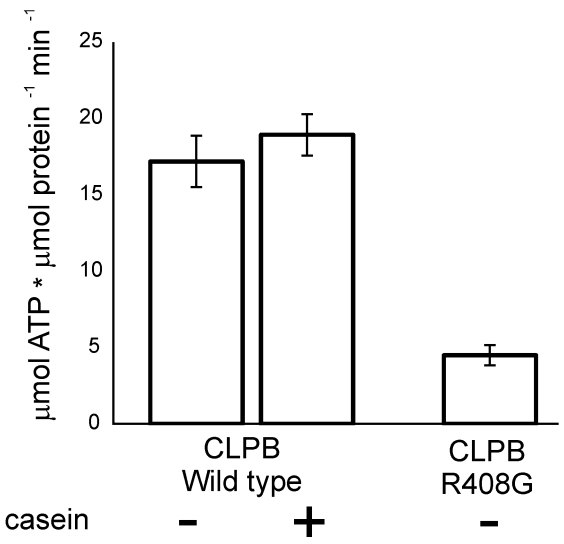

ATPase activity of purified wildtype and p.Arg408Gly (p.R408G) ClpB. All measurements were run in triplicate. Mutant ClpB had 26% ATPase activity compared to wild type human ClpB.

Table S1. Primer sequences for Sanger Sequencing of *CLPB* (NM_030813.4)

Exon	Forward primer (5'→3')	Reverse primer (5'→3')
1	caggaaacagctatgaccGGCAGCCATGTTGGACGTGG	tgtaaaacgacggccagtAGTTAGGACAATCTTCCCGCC
2	caggaaacagctatgaccGTACTGCCACTGTCTTAGTGG	tgtaaaacgacggccagtTCCAAAGCAAAGTCATCACACG
3	caggaaacagctatgaccCACACCAGGTGGGAGAGTGC	tgtaaaacgacggccagtCAGATGTCAAGCCATACACTG
4	caggaaacagctatgaccTCCGGATCTGGGTCTGTACC	tgtaaaacgacggccagtACAGAGGTAAAGAACATGCAGG
5	caggaaacagctatgaccTCTGGGGGTAGAGGGCTTGG	tgtaaaacgacggccagtAAAGAGATAGTCAGATGAGACC
6	caggaaacagctatgaccGGAGGATAACAGGGCTCTGG	tgtaaaacgacggccagtTGCCTCTTCTTACCCAGCAC
7	caggaaacagctatgaccGAAATCAGAGCCTTAAGCCACC	tgtaaaacgacggccagtAGTGAAGGATTAAATGATGCATGG
8	caggaaacagctatgaccCTATGAAGCAGGACCCCTGG	tgtaaaacgacggccagtATCCAGTTTGGTGACGACAGG
9	caggaaacagctatgaccATACTTAGTGATAATTATCCTGCC	tgtaaaacgacggccagtGGAGGCCGTTGCTTTTAGAGC
10	caggaaacagctatgaccTGCGCCTCAACATTCTCATCC	tgtaaaacgacggccagtTTCAGAGGGTCAGATTTTTTGGG
11	caggaaacagctatgaccGGGATAGTTGAGGTGCTCTCC	tgtaaaacgacggccagtTGAGGCCCAAATGACAAGACC
12	caggaaacagctatgaccTCTCTGTTGAGAGAGGCAACC	tgtaaaacgacggccagtGAATGACCAGCTAGCCTCTGG
13	caggaaacagctatgaccGGAGGTGAGAACTGAGAGTGC	tgtaaaacgacggccagtAGCTAGGGACAGAGCTGCCC
14	caggaaacagctatgaccTTTCCATGGGCAGGCCAAGG	tgtaaaacgacggccagtGGCTTCCAGATCTTTAGGATGG
15-16	caggaaacagctatgaccTGGTAATTTCCCTAACCCGC	tgtaaaacgacggccagtCAAGCTATAGGGAGGCAGGC
17	caggaaacagctatgaccGGTCTCTGAGTTGCCCTAGC	tgtaaaacgacggccagtAGGCCTGAGACTGGGTAGAG

Overview of the PCR primers used to amplify the exons of the *CLPB* gene (NM_030813.4). All primers contained a M13 sequence at the 5'end that allowed for sequencing of the PCR products using universal M13 primers.

Table S2. Primer sequences of primers used for QPCR analysis of *CLPB* (NM_030813.4)

	Forward primer (5'→3')	Reverse primer (5'→3')
GUSB (NM_000181.1)	agagtggtgctgaggattgg	ccctcatgctctagcgtgtc
PPIB (NM_000942.4)	cggaaagactgttccaaaaac	gattacacgatggaatttgctg
CLPB (NM_030813.4)	tgaataaagaaatgtaaagg	ttaataaattaaaattatag

Table S3. Oxidative phosphorylation measurements in muscle and cultured fibroblasts

	parameter	Individual 6	Individual 9	reference value	unit
muscle	ATP + CrP production rate	28,8	ND	15.4 - 30.2	nmol ATP.h^{-1}.(mU CS)$^{-1}$
	pyruvate oxidation rate	3,01	1,96	1.74 - 3.11	nmol CO_2.h^{-1}.(mU CS)$^{-1}$
	complex I	69	102	47 - 154	mU.(mU CS)-1
	complex II	247	230	134 - 354	mU.(mU CS)-1
	complex III	954	969	696 - 1756	mU.(mU CS)-1
	complex IV	1381	1189	470 - 1842	mU.(mU CS)-1
	complex V	358	349	161 - 711	mU.(mU COX)-1
	complex II+III	347	308	176 - 492	mU.(mU CS)-1
	citrate synthase	238	187	84 - 365	mU.(mg protein)-1
fibroblasts	complex I	342	318	163 - 599	mU.(mU CS)-1
	complex II	465	435	335 - 888	mU.(mU CS)-1
	complex III	850	694	570 - 1383	mU.(mU CS)-1
	complex IV	604	537	288 - 954	mU.(mU CS)-1
	complex V	711	635	193 - 819	mU.(mU CS)-1
	complex II+III	267	263	128 - 534	mU.(mU CS)-1
	citrate synthase	302	370	151 - 449	mU.(mg protein)-1

ND = not determined.

OXPHOS measurements in different tissues were performed as reported earlier. The measurement of the oxygen consumption rate in the presence of pyruvate and malate as mitochondrial respiration substrates was performed as described previously [1].

Table S4. Direct interaction partners of CLPB as identified by database searches.

	Database	Method	Reference
COPS6	STRING	Affinity Capture-MS	[9]
COPS6	BioGRID		
CUL3	BioGRID	Affinity Capture-MS	[10]
ERCC6L	BioGRID	Affinity Capture-MS	Huttlin EL (2014/pre-pub)
HDAC11	BioGRID	Affinity Capture-MS	[11]
IRS4	BioGRID	Affinity Capture-Luminescence	[12]
IRS4	BioGRID	Affinity Capture-MS	[12]
MDFI	IntAct	Two-hybrid	[13]
MDFI	BioGRID		
MGEA5	BioGRID	Affinity Capture-MS	*
OSBPL10	STRING	Affinity Capture-MS	[9]
SMAD9	HPRD	Two-hybrid	[14]
SMAD9	IntAct		
SMAD9	MINT		
TERF2	BioGRID	Affinity Capture-MS	[15]
TSEN2	BioGRID	Affinity Capture-MS	*
TTF2	HPRD	Affinity Capture-MS	*
TTF2	STRING	Two-hybrid	[16]
UBC	BioGRID	Affinity Capture-MS	[17]
UCHL3	STRING	Affinity Capture-MS	[9]
UCHL3	BioGRID	Affinity Capture-MS	*
USP30	STRING	Affinity Capture-MS	Sowa ME (2009)
USP30	BioGRID		
RG9MTD1	STRING	CoIP	[18]
STIP1	STRING	CoIP	[19]

* http://thebiogrid.org/166968/publication/high-throughput-proteomic-mapping-of-human-interaction-networks-via-affinity-purification-mass-spectrometry.html (Huttlin EL et al. High throughput proteomic mapping of human interaction networks via affinity-purification mass spectrometry (pre-publication)).Data on proteins that physically interact with CLPB (**Table S4**) were retrieved from public databases (BioGRID, Biological General Repository for Interaction Datasets; HPRD, Human Protein Reference Database; MINT, Molecular Interactions Database; STRING, Search Tool for the Retrieval of Interacting Genes/Proteins). Database information on physical protein interactions for HAX1 was obtained from the most recent release from the BioGRID database (www.thebiogrid.org/download.php; compiled on October 25th 2014).

In addition, a live cell protein interaction screen of CLPB against a library of *n* = 100 proteins was performed using bioluminescence resonance energy transfer (BRET), as described before[4; 5]. Briefly, we generated a protein library enriched for gene ontology (GO) tags linked to functions and processes that are associated with 3-MGA-uria[6; 7]. Proteins were selected from a library of n > 500 proteins based on the number of associations with GO biological_process (phospholipid biosynthetic process, cholesterol homeostasis, lipid metabolic process, response to calcium ion, calcium ion binding, membrane organization) and GO cellular_component (endoplasmic reticulum, mitochondrion, peroxisome, Golgi apparatus, integral to membrane).

Table S5. Proteins interacting with CLPB as determined by BRET.

#	Interaction partner	BRET pair		BRET Ratio	
	Name	*Protein 1*	*Protein 2*	*1st experiment*	*2nd experiment*
1	ABCD4	CLBP-C-Venus	ABCD4-C-hRluc	0,019	0.035 *
2	AGXT	CLBP-C-Venus	AGXT-C-hRluc	0.028 *	0.037 *
3	ATP2A2	CLBP-N-Venus	ATP2A2-N-hRluc	0.028 *	0,000
4	CARD8	CLBP-N-Venus	CARD8-N-hRluc	0.051 *	0.059 *
5	CYB5	CLBP-N-hRluc	CYB5-C-Venus	0,020	0.027 *
6	FAR1	CLBP-N-hRluc	FAR1-C-Venus	0,013	0.027 *
7	FASN	CLBP-N-hRluc	FASN-N-Venus	0,013	0.027 *
8	FIS1	CLBP-N-hRluc	FIS1-C-Venus	0.055 *	0.033 *
9	HMGCL	CLBP-C-Venus	HMGCL-C-hRluc	0,000	0.029 *
10	IL1B	CLBP-N-hRluc	IL1B-N-Venus	0.027 *	0,026
11	MIF	CLBP-N-hRluc	MIF-C-Venus	0.051 *	0,025
12	MPV17L2	CLBP-N-hRluc	PEX19-N-Venus	0.050 *	0.062 *
13	NLRP2	CLBP-N-hRluc	PEX5isob-N-Venus	0.056 *	0.054 *
14	PEX19	CLBP-N-hRluc	PYCARD-C-Venus	0.062 *	0.057 *
15	PEX5isob	CLBP-N-hRluc	RIPK2-N-Venus	0.030 *	0,025
16	PYCARD	CLBP-N-Venus	SSR1-C-hRluc	0,000	0.037 *
17	RIPK2	CLBP-N-Venus	MPV17L2-N-hRluc	0.037 *	0,000
18	SSR1	CLBP-N-hRluc	NLRP2-N-Venus	0.030 *	0,002
19	SERAC1	SERAC1-N-Venus	CLBP-N-hRluc	0.028 *	0.027 *

A live-cell screen of CLPB against a library of 100 proteins by means of bioluminescence resonance energy transfer (BRET) identified 19 positive interactions. The library of 100 proteins was derived from a random library by enrichment for proteins associated with the Gene Ontology (GO) annotations biological_processes phospholipid biosynthetic process, cholesterol homeostasis, lipid metabolic process, response to calcium ion, calcium ion binding, membrane organization, and GO cellular_components endoplasmic reticulum, mitochondrion, peroxisome, Golgi apparatus, integral to membrane. The protein interaction pairs are given and the orientation (C, C-terminus; N, N-terminus) of BRET tags (Venus, variant of yellow fluorescent protein; Rluc, Renilla luciferase) is indicated. Protein interactions were assumed as true positive, if the BRET ratio of at least one experiment exceeded a method specific threshold of 0.0263 (indicated by *).

BRET protein-protein interaction assays were performed in transfected COS-7 cells as described before[4; 5]. Full-length open reading frames of genes encoding CLPB (BC 006404.2) and genes encoding proteins of the $n = 100$ library were introduced into plasmid vectors for

the expression of amino- and carboxy-terminal fusions with Rluc or YFP. All eight possible combinations of Rluc (donor) or YFP (acceptor) fusions tagged at the amino or carboxyl terminus were tested in duplicates for each putative interaction pair at an acceptor/donor ratio of 3:1. BRET ratios were calculated by the equation $R = (I_A / I_D) - cf$, where R is the BRET ratio, I_A is the BRET signal, I_D is the Rluc signal and cf is a correction factor ($(I_A / I_D)_{control}$), with co-transfection of the donor fusion protein with YFP in the absence of the second protein of interest used as the control. Protein interactions were assumed to be true positive, if the BRET ratio of at least one combination of acceptor and donor tagged interaction pairs exceeded a method-specific threshold of 0.0263. The threshold for classification of positive protein interactions was generated by measurement of two libraries of $n = 60$ proteins with known positive protein interactions (positive reference set, PRS) and putatively negative protein interactions (random reference set, RRS), as described previously [8].

References

1. Rodenburg, R.J. (2011). Biochemical diagnosis of mitochondrial disorders. Journal of inherited metabolic disease 34, 283-292.
2. Rakovic, A., Grunewald, A., Kottwitz, J., Bruggemann, N., Pramstaller, P.P., Lohmann, K., and Klein, C. (2011). Mutations in PINK1 and Parkin impair ubiquitination of Mitofusins in human fibroblasts. PloS one 6, e16746.
3. Houtkooper, R.H., Rodenburg, R.J., Thiels, C., van Lenthe, H., Stet, F., Poll-The, B.T., Stone, J.E., Steward, C.G., Wanders, R.J., Smeitink, J., et al. (2009). Cardiolipin and monolysocardiolipin analysis in fibroblasts, lymphocytes, and tissues using high-performance liquid chromatography-mass spectrometry as a diagnostic test for Barth syndrome. Analytical biochemistry 387, 230-237.
4. Bakele, M., Lotz-Havla, A.S., Jakowetz, A., Carevic, M., Marco, V., Munta, A.C., Gerstin, S.W., and Hartl, D. (2014). An interactive network of elastase, secretases, and PAR-2 protein regulates CXCR1 receptor surface expression on neutrophils. The Journal of biological chemistry 289, 20516-20525.
5. Gersting, S.W., Lotz-Havla, A.S., and Muntau, A.C. (2012). Bioluminescence resonance energy transfer: an emerging tool for the detection of protein-protein interaction in living cells. Methods in molecular biology (Clifton, NJ) 815, 253-263.
6. Wortmann, S.B., Duran, M., Anikster, Y., Barth, P.G., Sperl, W., Zschocke, J., Morava, E., and Wevers, R.A. (2013). Inborn errors of metabolism with 3-methylglutaconic aciduria as discriminative feature: proper classification and nomenclature. Journal of inherited metabolic disease 36, 923-928.
7. Wortmann, S.B., Espeel, M., Almeida, L., Reimer, A., Bosboom, D., Roels, F., de Brouwer, A.P., and Wevers, R.A. (2014). Inborn errors of metabolism in the biosynthesis and remodelling of phospholipids. Journal of inherited metabolic disease.
8. Braun, P., Tasan, M., Dreze, M., Barrios-Rodiles, M., Lemmens, I., Yu, H., Sahalie, J.M., Murray, R.R., Roncari, L., de Smet, A.S., et al. (2009). An experimentally derived confidence score for binary protein-protein interactions. Nature methods 6, 91-97.
9. Sowa, M.E., Bennett, E.J., Gygi, S.P., and Harper, J.W. (2009). Defining the human deubiquitinating enzyme interaction landscape. Cell 138, 389-403.
10. Bennett, E.J., Rush, J., Gygi, S.P., and Harper, J.W. (2010). Dynamics of cullin-RING ubiquitin ligase network revealed by systematic quantitative proteomics. Cell 143, 951-965.
11. Joshi, P., Greco, T.M., Guise, A.J., Luo, Y., Yu, F., Nesvizhskii, A.I., and Cristea, I.M. (2013). The functional interactome landscape of the human histone deacetylase family. Molecular systems biology 9, 672.
12. Taipale, M., Tucker, G., Peng, J., Krykbaeva, I., Lin, Z.Y., Larsen, B., Choi, H., Berger, B., Gingras, A.C., and Lindquist, S. (2014). A quantitative chaperone interaction network reveals the architecture of cellular protein homeostasis pathways. Cell 158, 434-448.
13. Venkatesan, K., Rual, J.F., Vazquez, A., Stelzl, U., Lemmens, I., Hirozane-Kishikawa, T., Hao, T., Zenkner, M., Xin, X., Goh, K.I., et al. (2009). An empirical framework for binary interactome mapping. Nature methods 6, 83-90.
14. Colland, F., Jacq, X., Trouplin, V., Mougin, C., Groizeleau, C., Hamburger, A., Meil, A., Wojcik, J., Legrain, P., and Gauthier, J.M. (2004). Functional proteomics mapping of a human signaling pathway. Genome research 14, 1324-1332.
15. Giannone, R.J., McDonald, H.W., Hurst, G.B., Shen, R.F., Wang, Y., and Liu, Y. (2010). The protein network surrounding the human telomere repeat binding factors TRF1, TRF2, and POT1. PloS one 5, e12407.
16. Leonard, D., Ajuh, P., Lamond, A.I., and Legerski, R.J. (2003). hLodestar/HuF2 interacts with CDC5L and is involved in pre-mRNA splicing. Biochemical and biophysical research communications 308, 793-801.
17. Stes, E., Laga, M., Walton, A., Samyn, N., Timmerman, E., De Smet, I., Goormachtig, S., and Gevaert, K. (2014). A COFRADIC protocol to study protein ubiquitination. Journal of proteome research 13, 3107-3113.

18. Holzmann, J., Frank, P., Loffler, E., Bennett, K.L., Gerner, C., and Rossmanith, W. (2008). RNase P without RNA: identification and functional reconstitution of the human mitochondrial tRNA processing enzyme. Cell 135, 462-474.
19. Behrends, C., Sowa, M.E., Gygi, S.P., and Harper, J.W. (2010). Network organization of the human autophagy system. Nature 466, 68-76.
20. Biasini, M., Bienert, S., Waterhouse, A., Arnold, K., Studer, G., Schmidt, T., Kiefer, F., Cassarino, T.G., Bertoni, M., Bordoli, L., et al. (2014). SWISS-MODEL: modelling protein tertiary and quaternary structure using evolutionary information. Nucleic acids research 42, W252-258.
21. Lee, S., Sowa, M.E., Watanabe, Y.H., Sigler, P.B., Chiu, W., Yoshida, M., and Tsai, F.T. (2003). The structure of ClpB: a molecular chaperone that rescues proteins from an aggregated state. Cell 115, 229-240.
22. Mogk, A., Schlieker, C., Strub, C., Rist, W., Weibezahn, J., and Bukau, B. (2003). Roles of individual domains and conserved motifs of the AAA+ chaperone ClpB in oligomerization, ATP hydrolysis, and chaperone activity. The Journal of biological chemistry 278, 17615-17624.
23. Leidhold, C., von Janowsky, B., Becker, D., Bender, T., and Voos, W. (2006). Structure and function of Hsp78, the mitochondrial ClpB homolog. Journal of structural biology 156, 149-164.
24. Biter, A.B., Lee, S., Sung, N., and Tsai, F.T. (2012). Structural basis for intersubunit signaling in a protein disaggregating machine. Proceedings of the National Academy of Sciences of the United States of America 109, 12515-12520.
25. Pfaffl, M.W. (2001). A new mathematical model for relative quantification in real-time RT-PCR. Nucleic acids research 29, e45.
26. Livak, K.J., and Schmittgen, T.D. (2001). Analysis of relative gene expression data using real-time quantitative PCR and the 2(-Delta Delta C(T)) Method. Methods (San Diego, Calif) 25, 402-408.